APPROVAL SHEET

Title of Thesis: Development of Computational Image Processing Algorithms for Detecting Morphological Features of Melanoma

Name of Candidate: Alireza Chamani

Master of Science, 2014

Thesis and Abstract Approved:

Dr. Liang Zhu

Professor

Department of Mechanical Engineering

University of Maryland, Baltimore County

Date Approved: Nov. 21, 2014

Curriculum Vitae

Alireza Chamani

Qualification Highlights

- Graduate level research and professional experience with Design, Modelling and FEM concepts using COMSOL Multi-Physics, Autodesk Packages, Pro-E and Solidworks
- Design and Execution of Several HVAC projects from scratch to implementation; engaged in all phases of conceptual, preliminary and detailed design using AutoCAD BIM, installations and testing. Hands-on experience in Site Investigation, Cost Estimation and Budgeting, Thermal Load Calculation and Equipment Selection.
- Managed team of construction, mechanical and electrical engineers in large-scale industrial construction projects; engaged in Planning, Execution and Controlling phases. Strong Analytical Problem-Solver and able to anticipate unplanned risks and opportunities.

Education

University of Maryland-Baltimore County, Baltimore, MD 2012 - 2014
Master of Science: Mechanical Engineering-Biomechanics
M.Sc. Thesis: Development of Computational Image Processing Algorithms for Detecting Morphological Features of Melanoma

Amirkabir University of Technology, Tehran, Iran 2006 - 2011
Bachelor of Science: Mechanical Engineering
B.Sc. Project: Prototyping and Experimental Analysis of Fiber-Metal Composites with Thermoplastic Matrix (GLARE Composites)

Certifications

Project Management Professional (PMP) Jul 2013
Certified through Project Management Institute (PMI)

Professional Experience

Project Manager 2013 - Present

AEGIS Mechanical Corporation, Baltimore, MD

- Estimated and led the bidding process for multiple projects ranging from $50,000 to $750,000
- Calculated thermal load and sized heating and cooling equipment for industrial projects
- Engaged in writing proposals, securing contracts, evaluating project progress, cost and schedule analysis, awarding sub-contracts and procurements for
    - Clifton Mansion Restorations
    - University of Maryland – Baltimore Renovations
    - Johns Hopkins University – Latrobe Hall
    - Johns Hopkins Hospital – Bloomberg CT Scan
    - BGE – Russett & Tipton

Graduate Teaching Assistant 2012 - 2014

University of Maryland-Baltimore County, Baltimore, MD

- Instructed "Thermodynamics" course covering 1st and 2nd laws, Enthalpy and Entropy, Steam and Gas Power Cycles, Heating and Refrigeration and Exergy

Graduate Research Assistant 2012 - 2014

University of Maryland-Baltimore County, Baltimore, MD

- Conducted a clinical research for FDA verifying the accuracy of the clinical digital thermometers in a 400-patients study
- Developed a "Melanoma Detection" MATLAB function. The function analyzes an image of the skin as the input and using image-processing methods evaluates the probability of melanoma
- Modeled and analyzed heat generation due to friction in an artificial joint for FDA using COMSOL Multi-Physics package

Assistant Project Manager/Intern Aug 2013 – Dec 2013

General Dynamics Information Technology, Towson, MD

- Planned for demolition, construction, furniture design and installation and relocation process for Towson Renovation Phase III

- Produced project charter, led the requirements collection meeting, created WBS and produced the schedule with MS Project based on the signed WBS. Designed a plan for project control and change management.

Assistant Project Manager/Lead HVAC Designer Jul 2008 – Sep 2011
Ross Co., Tehran, Iran

- Directed the planning, construction, purchases, and tests as the "on-site" construction project manager of 540-bed teaching hospital in Zahedan-Iran with a total budget of $12 million. Managed to meet all the requirements and provide all deliverables proposed by the government within the deadline and budget organizing the construction, mechanical, electrical and technical teams.
- Eliminated the traditional interactions and evolved the company into cloud-based shared documents using Google Apps. Designed and managed the company's website and data servers. Initiated PMI-based trainings for the new project managers within the company using PrimeLearning online courses.

Computer Skills

Software Packages

- Solidworks, Catia, COMSOL Multiphysics, ANSYS (CFD and Solid), AutoCAD Pro Suite, Carrier, Pro-Engineer
- MS Office (Word, Excel, Access, PowerPoint, Visio), MS Project

Programming

- MATLAB, C, Pascal, HTML, Jscript

OS

- DOS, Windows, Mac OS

Publications

Theoretical Simulation of Temperature Elevations in a Joint Wear Simulator During Rotation
ASME Journal of Biomechanical Engineering Oct 2013

Testing Image Processing Algorithms for Melanoma Detection
ASME Bio-Engineering Conference (SBC 2013) Jun 2013

Abstract

This thesis research is focused on advancing image processing techniques and algorithms used for detecting skin melanoma. We have modified previous image processing approaches and developed computational algorithms for quantifying morphological features of a mole image. Applying the algorithms to 20 mole images downloaded from educational websites, we have identified three cut-off ratios to distinguish melanoma images from benign mole images. More specifically, the higher the boundary irregularity ratio, and/or the asymmetry ratio, and/or the color variation ratio, the high chance the mole is melanoma leading. The irregularity ratio cutoff is identified as 1.96, suggesting 96% more circumference length than that of a circle with the same area. One finds that the cut-off ratio for assessing asymmetry of the mole image is 0.109, representing the degree of asymmetry as approximately 11% to place a mole image into the melanoma group. Evaluation of the color variation of the moles leads to a cut-off ratio of the color variation as 0.334. Statistical analyses have been performed to determine the confidence of cut-off ratios, varying from 63% to 81%, for placing a mole image into its correct groups. The algorithms have also been implemented to assess "changes" of mole images over time observed by a dermatologist. Using a ±14% as the definition of changes, the algorithm identifies 9 of the 10 mole images as changed over time. Among the irregularity, asymmetry, color variation, and size ratios, 5 out of the 9 moles have shown changes in one ratio, 2 out the 9 moles have experience changes in two ratios, 1 mole has shown changes in three ratios, and only 1 mole shows changes in all four ratios. The computational results are consistent with the general observations that

human eyes are sensitive to size changes and color variation changes, and may not be very good to distinguish changes in border irregularity and asymmetry. The developed algorithms can be helpful to assist a physician in evaluating subtle changes of mole images that may not be very sensitive to the eyes.

DEVELOPMENT OF COMPUTATIONAL IMAGE PROCESSING ALGORITHMS FOR DETECTING MORPHOLOGICAL FEATURES OF MELANOMA

By

Alireza Chamani

Thesis submitted to the Faculty of the Graduate School of the
University of Maryland, Baltimore County, in partial fulfillment
of the requirements for the degree of
Master of Science

2014

ProQuest LLC.
789 East Eisenhower Parkway
P.O. Box 1346
Ann Arbor, MI 48106 - 1346

Dedication

To my father, Mohammad Hassan, my “engineer” idol; the only cause and purpose of what I am and where I am standing today. My greatest support in every single step and the dream role model whom I had the privilege of knowing and having in every moment.

To my mother, Maliheh, my symbol of “caring”; who had to see, hear and “feel” every single thing that would happen all across the world, just to assure me that “nothing has changed, it’s all the same, and you just focus ahead”

To my wife, Mahsan, my “present and future”; my companion, my soul-mate, the “moon and the sun” of my life, the beauty whose sole smile paints the most amazing moments, unforgettable ones.

Acknowledgements

I would like to begin my acknowledgement by thanking my advisor professor, Dr. Liang Zhu, for giving me the opportunity to work in the Bio-Heat Transfer lab at UMBC. Her generous support, knowledge and guidance made me able to complete this research. I managed to develop and improve my research and teaching skills using her guidelines, and I greatly appreciate her patience and support for helping me to write and edit this thesis. I would like to thank my thesis committee; Dr. Ronghui Ma and Dr. Carlos Romero-Talamas, for taking the time to read my thesis and providing insightful remarks. I thank the staff at Mechanical Engineering Department, especially Mr. Chuck Smithson, for their help and assistance during my study at UMBC. My graduate study was supported by Mechanical Engineering Department at UMBC and Food and Drug Administration. I would like to thank my dear friend, Barnett Carroll, his family-like care and support had a significant impact on my research. And last but not least, my dear family, their love and support gave me the energy and purpose to accomplish this project.

Table of Contents

List of Figures

List of Tables

Chapter 1

Literature Review and Specific Aims

Current melanoma researches have been focused on understanding skin structure, locations and pathology of cells prone to producing tumors, and developments of diagnosis tools and treatment methods. In this chapter, background information and literatures relevant to melanoma diagnoses and treatments are reviewed and discussed. The chapter concludes with a summary of all the sections discussed to illustrate limitations and motivations of this thesis research.

1.1 Melanoma Basics

The terms "melanoma" and "skin cancer" are often erroneously used interchangeably. There are three common skin cancers: basal cell carcinoma, squamous cell carcinoma, and melanoma. Basal and squamous cell carcinomas account for the majority of skin cancers diagnosed in the United States. Both cancer types respond well to treatment [1, 2]. Unfortunately, the third one, melanoma, is often lethal, contributing to more than 79% of all skin cancer fatalities. It is the 5th leading cause of cancer-related death in the United States. Treatment outcomes of melanoma are very poor, with a post-metastasis survival rate of 15%, according to data provided by the American Cancer Society [3].

1.1.1 Definition and Formation of Melanoma

The most dangerous type of skin cancer is melanoma. It mostly occurs in the skin; and less frequently in the eye, nose, mouth or genitals. The word "melanoma" consists of two Greek words: *melas* (meaning black) and *oma* (meaning tumor). Even though melanoma is the least common skin cancer and only accounts for 4% of the cases, it is responsible for 79% of all skin cancer deaths [4].

At early stages of melanoma, the cancerous cells start to develop rapidly and form tumors due to damaged DNA, possibly by ultraviolet radiation from the sun and tanning beds. The skin tumors mainly develop in "pigment-producing" melanocytes, which are located in the basal layer of the epidermis, as shown in Figure 1.1 [5, 6].

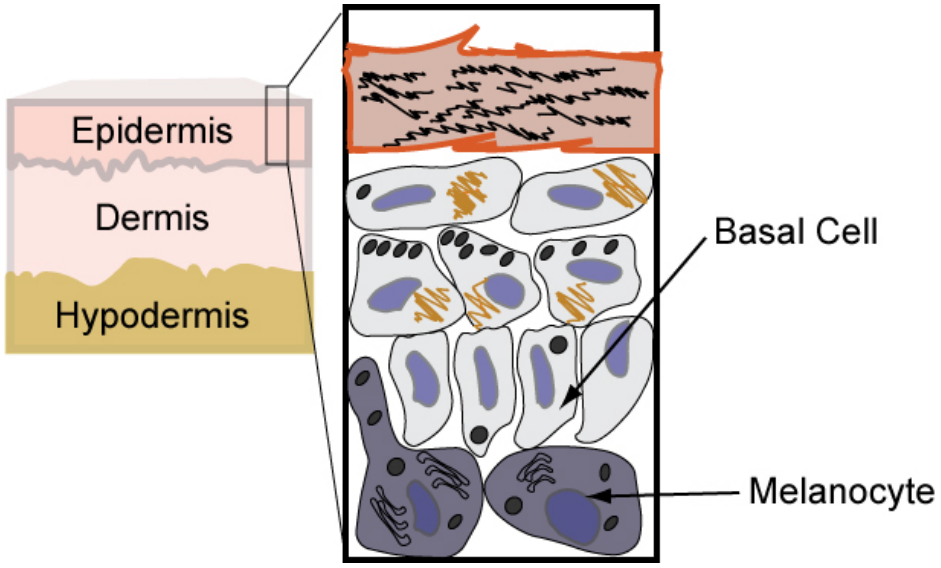

Figure 1-1 Melanocytes (pigment producing cells) in an epidermis layer [7].

Melanoma starts in "melanocytes", cells producing melanin. Melanin is a brown-black pigment that determines the color of the skin, eyes and hair in the humans, but its

main purpose is to protect nuclei of the skin cells against the UV radiation, shown in Figure 1-2 [8]. Melanin produced in melanocytes is carried in small packets called "melanosome" to keratinocyte where they are placed on top of the nuclei to block the UV rays. When being exposed to high UV radiations, the double bonds in the DNA of melanocytes may be separated. The separation of the bonds allows the nearby molecules to react. If two UV-modified thymine-base molecules are adjacent to each other on a single strand of DNA, they form a "thymine dimer" as a result of covalent bonding. Usually this initial bond causes the two nearby bases to form a bond making a four-membered ring. If damage caused by UV radiation is not corrected by molecular repairing mechanisms, DNA replication and transcription are blocked and genetic information will be permanently mutated. The outcome varies in a range from a normal melanocyte to invasive metastatic melanoma that is not easily treated. Generally, melanomas that are diagnosed during the *radial growth phase* have shown excellent prognosis, but after the *deep growth phase* starts, the chance of finding a cure is close to zero. Even though melanoma cells may have various colors and sizes, they appear mostly black or brown [9-11].

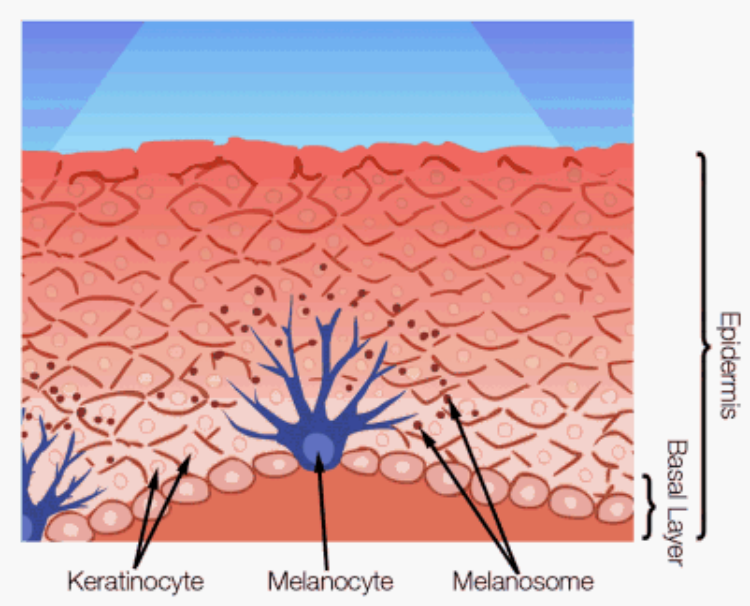

Figure 1-2 The melanin contained in melanomes moves to keratinocyte [12].

1.1.2 Types

In general, there are three types of melanoma. Cutaneous melanoma is the most common type of melanoma and occurs on the skin. Mucosal melanoma is a rare type and occurs in the mucous membranes, such as nose, throat, vagina, anus, and mouth. Ocular melanoma is another rare form that only occurs in the eye. [13]

Cutaneous melanoma is the main focus of this research. Most cutaneous melanomas begin only in the outer layer of the skin. It can be invasive from its initial formation to the inner skin layers. The deeper the invasive cells penetrate, the more lethal the disease becomes, since the tumor becomes more prone to spreading to the other parts of the body [13, 14]

Figure 1-3 shows four different types of cutaneous melanoma. Superficial spreading melanomas (Figure 1-3a), which are found in more than 70 percent of the

cases, located in the top layer of the skin for a long time before starting to penetrate into deep layers. It appears as a patch with irregular borders and with an asymmetrical shape. The color inside the lesion varies between brown, black, red and white. Superficial spreading melanomas are seen mostly in the trunk area (men), in the legs (women), and the upper chest area (men and women) [15].

Lentigo maligna melanomas (Figure 1-3b) are similar to superficial melanomas. It remains close to the surface and appears mostly in darker colors. Lentigo maligna melanomas are mostly diagnosed in elderly and in parts of the skin that are damaged by sun exposure through time, and they are seen on the face, ears, arms, and upper torso [14, 16].

Acral lentiginous melanomas (Figure 1-3c) have different properties compared to the other two types. It mostly appears under the nails with dark colors. This type is most common in African-Americans and Asians [14].

Nodular melanomas (Figure 1-3d) are the most dangerous and aggressive type of melanoma and they have become invasive when they are diagnosed. The most common color for this type is black but it may appear in other colors like blue, gray, brown, white or skin tone as well. The most probable locations of this type are on legs, arms, torsos, and scalps [14, 16].

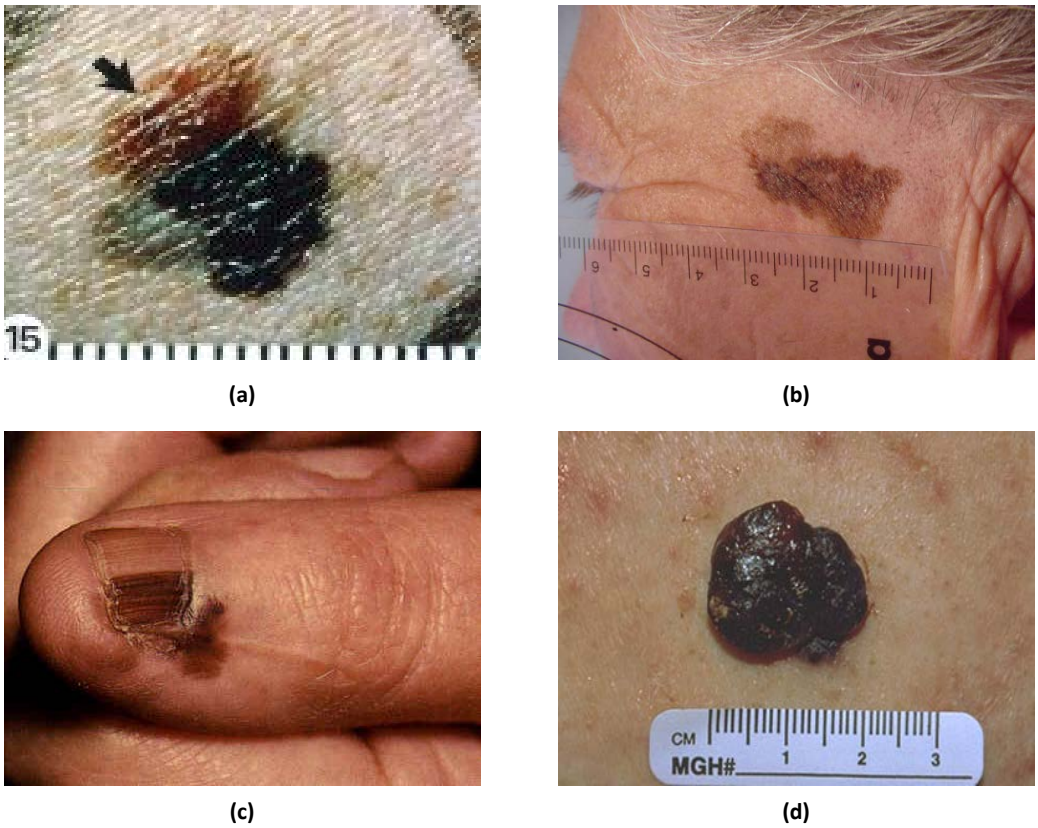

Figure 1-3 Four types of cutaneous melanoma: (a) Superficial Spreading Melanoma [15], (b) Lentigo Maligna [17], (c) Acral Lentiginous [18] and (d) Nodular Melanoma [19].

1.2 Statistics and Facts

Based on the statistics collected in 2014, skin melanoma contributes to the 5th most common cancer cases in the United States [20]. According to Table 1-1, more than 57% of the estimated melanoma cases in 2014 will be in men. Approximated 13% of the diagnosed melanoma cases will lead to death of the patients [21].

Table 1-1 The most Common Cancer Cases (2014 Estimates) [22].

Most Common Types of Cancer Cases	Men	Women	Total
1. Prostate	233,000	-	233,000
2. Breast	-	232,670	232,670
3. Lung and Bronchus	116,000	108,210	224,210
4. Colon and Rectum	71,830	65,000	136,830
5. Melanoma	**43,890**	**32,210**	**76,100**
6. Bladder	56,390	18,300	74,690
7. Non Hodgkin Lymphoma	38,270	32,530	70,800
8. Kidney and Renal Pelvis	39,140	24,780	63,920
9. Endometrial	-	52,630	52,630
10. Thyroid	-	47,790	47,790

The most newly diagnosed cases of melanoma in 2013 were among patients of age from 55 to 64 (Figure 1-4). The median age at diagnosis was 61. The total number of diagnosed cases was 21.1 per 100,000 men and women in 2013. The fatality rates from melanoma were high in the middle-aged and elderly populations. More than 65% of the fatality cases were between 55 and 84 years old, shown in Figure 1-5. Melanoma is more common among individuals of fair complexion. According to the Surveillance, Epidemiology and End Results (SEER) Program of the National Cancer Institute, the diagnosed cases of melanoma have continuously increased in the past decades. It is possible that this is the consequence of the popularity of recreational tanning in the 1970s - 1990s affecting a generation of youth to intensive ultraviolet radiation. This may also be due to the continuous efforts from medical professionals for recommending routine or early screening for populations with high risks. On the plus side, the fatality rates have remained constant, setting an increasing trend of the survival rate [20, 23].

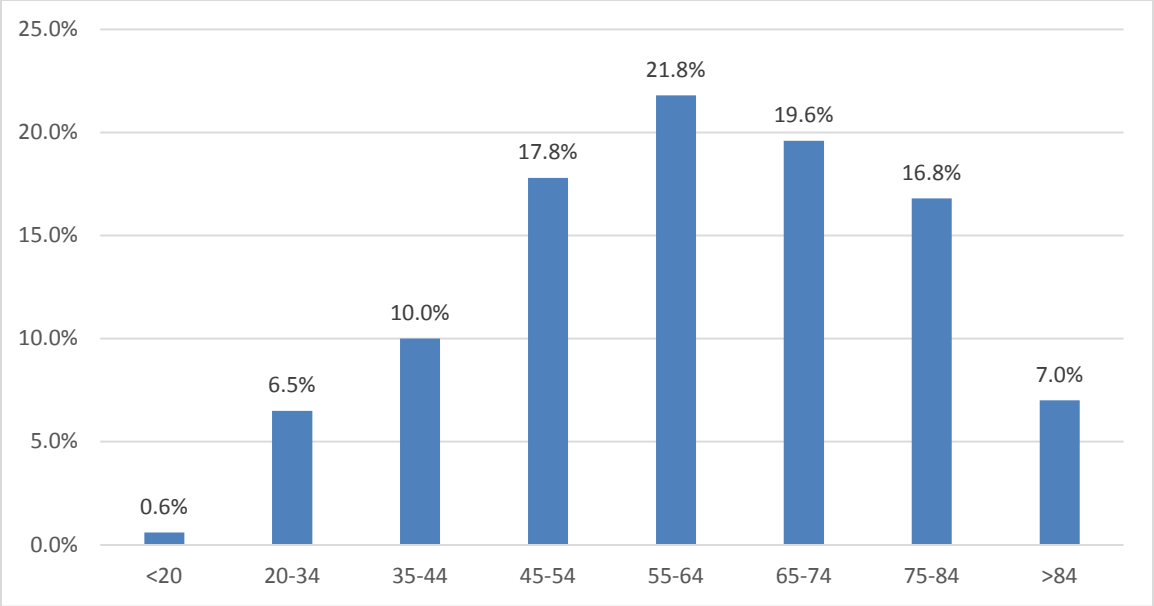

Figure 1-4 Percentages of new melanoma cases in 2013 by age groups [20].

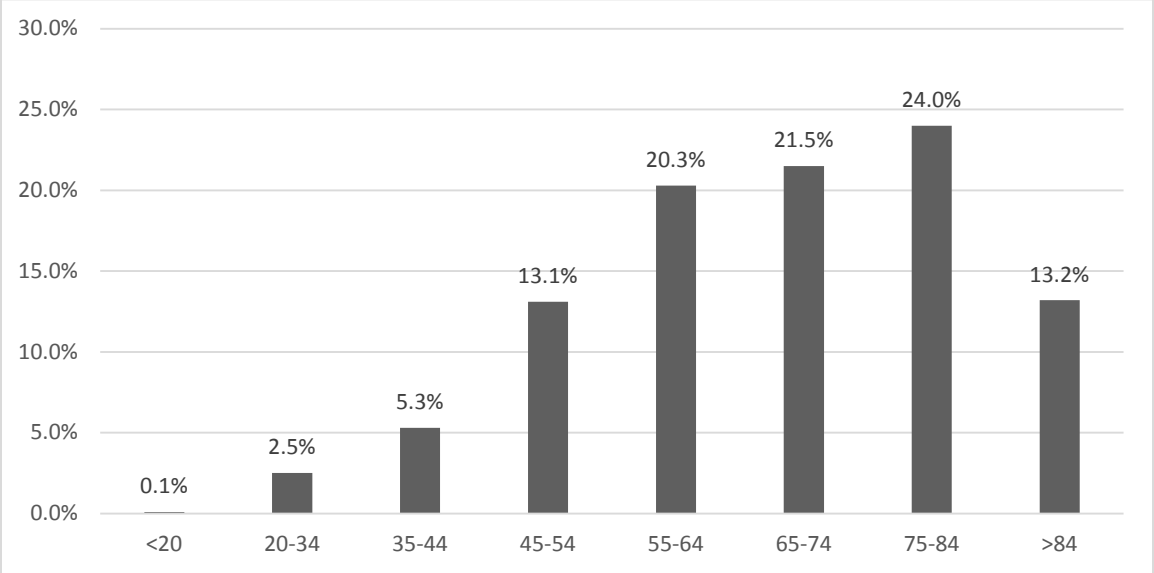

Figure 1-5 Percentages of deaths by melanoma in 2013 by age groups [20].

1.3 Medical Features

There are various risk factors for developing melanoma. One fact is that even though the level of risks is different for individuals, nobody is immune to it. Skin type and color, magnitude and duration of sun exposure, numbers of moles, and family history are the main factors that determine the risk of the disease [24].

1.3.1 Causes

People with lighter skin colors are more prone to melanoma and skin cancer in general. The number of people with pale skin who are diagnosed with melanoma is at least ten times higher than dark skinned patients. Moles do not generally increase the risk of melanoma; as a matter of fact, regular moles that are brown blemishes are safe for most people. Only atypical moles called “dysplastic nevi” are prone to becoming melanoma. UV rays can lead to development of melanoma. Blistering sunburns during childhood increase the risk. Cumulative exposure to low or moderate intensity of sunlight and UV rays is also a well-known cause of skin cancer. The popularity of recreational tanning in the 1970s-1990s exposed a generation of youth to intensive ultraviolet radiation, but sun exposure secondary to outdoor occupations has also contributed significantly to the development of skin cancer. In addition, a melanoma patient who is in remission is at a greatly increased risk of recurrence. Patients with a family history of melanoma are in great risks of invasive melanoma and need to see dermatologists more frequently than the general populations [25, 26].

1.3.2 Prevention Methods

The UV ray emitted from the sun is the main cause of skin cancer. It is possible to lower the absorbed UV by staying indoors on sunny days. Wearing sunglasses is effective too since they cover and protect eyes and the sensitive facial skin. Another simple yet effective means of protecting the skin is covering the body with clothing and a hat. Although it feels uncomfortable, it is crucial to wear long sleeve clothes on sunny days to cover as much skin as possible. There are different manufacturers that make UV protective clothes, which are stated effective in lowering the absorbed UV by the skin [27, 28].

The tanning beds are falsely advertised as UV free products to increase their sales. The truth is that the devices produce both UVA and UVB rays, which are extremely harmful for the skin and can lead to skin cancer in the long term. Researches show a direct link between tanning beds and risks of melanoma, especially if they are used before age of 30. Certain types of moles cause increased risks leading to melanoma. The first sign of melanoma is a change in size, shape or color of an existing mole. It is recommended to have those moles examined by a dermatologist, especially the ones that are “changing” and look unusual. Removing all moles on the skin is usually not a viable option.

There are tests available to detect the mutating genes that cause melanoma, although they are not perfectly accurate, and they are also costly. Sometimes these tests produce false positive diagnosis, and may complicate the process of diagnoses and treatments, as well as cause unnecessary panic. It is recommended to consult a genetic

counselor as well as having the moles checked by a dermatologist frequently, if the patients have a family history of melanoma [29].

1.3.3 Diagnosis

The routine annual office visits to a physician or dermatologist is a cost-effective step to diagnose skin melanoma. During a physical exam, the shape, color, size, and texture of moles on the skin are analyzed. Lymph nodes that are small collections of immune cells under the skin are targeted locations for melanoma. Enlarged lymph nodes may suggest presence of melanoma [30].

If a part of the skin is suspicious for melanoma, a tissue sample is resected from the location and analyzed under the microscope. Depending on the size of the infected area, different methods of biopsy are used. If the risk of melanoma is very low, “shave (tangential) biopsy” is used, and the top layers of the skin containing the epidermis are shaved with a surgical blade and then tested for melanoma. In “punch biopsy”, a deeper sample of the skin is removed using a device that looks like a round cookie cutter. The device is rotated to cut a sample containing dermis, epidermis and upper parts of subcutis. This method is often used when the risk of melanoma is high. To examine a tumor that has grown into deeper layers of skin, incisional or excisional biopsy is used. After numbing the area, the full thickness of the skin is cut using a surgical knife and a wedge of the skin is removed. Incisional biopsy removes only a part of the tumor whereas excisional biopsy removes the entire tumor. Biopsy may leave a scar on the surgical site.

Various imaging techniques can be used to diagnose spreading malignant cells. While this approach is not used on patients with an early-stage melanoma, it is significantly less invasive than biopsies. Chest x-ray is used to determine whether a melanoma has spread to lungs. In order to produce detailed images, Computer Tomography (CT) scan is used to detect enlarged lymph nodes. A CT scanner takes many pictures as it rotates around a body and the results are combined to produce a detailed three-dimensional image. Like CT scan, Magnetic Resonance Imaging (MRI) may distinguish tumors from its surrounding healthy organs or structures using strong magnetic fields. For melanomas in later stages, Positron Emission Tomography (PET) scan is used via injecting a radioactive substance to the body. Since the cancer cells are growing faster, they absorb most of the radioactive substance. The PET scanner produces images based on the radioactive emissions from the targeted tumors [31]. None of the above imaging techniques are suitable for melanoma diagnosis when the cancer has not spread to other parts of the body [32-34].

1.4 Previous Studies in Imaging Processing

An early and accurate diagnosis of melanoma has a great chance of successful treatment. Several studies have worked on developing an easy and widely accessible diagnosis method that can be used by non-professional individuals. Visual analysis of skin lesions has proven to be a promising initial step.

In order to conduct a detailed visual analysis, five distinctive features are investigated in the past, i.e., the ABCDE (Asymmetry, Boundary, Color, Diameter, and

Evolving) system. Typically, detecting the boundary of a mole is the first step to extract the lesion from the background. Then, how asymmetric and irregular the lesion is can be evaluated. In some studies, the color variation in a mole can be assessed. The size of a mole can be measured with a reference ruler and evaluation of mole evolutions over time is possible if the mole is photographed repeatedly over time.

For detecting of the border of a mole image, conventional edge detection methods like Sobel and Marr-Hildreth have been used. Sobel operator uses two *3x3* kernels to calculate the first and second derivatives along the horizontal and vertical directions of the mole (Figure 1-6). In the Marr-Hildreth approach, the image is convolved with the Laplacian operator of the Gaussian function to produce a fast approximation of the differentials. In principle, one way to find boundaries of objects is to detect discontinuities in pixel tonal values (*f*) at the edge of a region. The discontinuities can be mathematically quantified by the pixel tonal gradient:

$$\left|gradient\ of\ \ f\right| = \sqrt{\left(\frac{\partial f}{\partial x}\right)^2 + \left(\frac{\partial f}{\partial x}\right)^2} \qquad (1.1)$$

where the partial derivatives in the expression represent the rates of the total value changes in the horizontal and vertical directions of the image. A threshold operation is then applied to the image to segment the boundary pixels. In addition, the approach also leads to the identification of the patched regions with multi-colors. However, this approach strongly relies on how sharp the mole changes its color from its background [35].

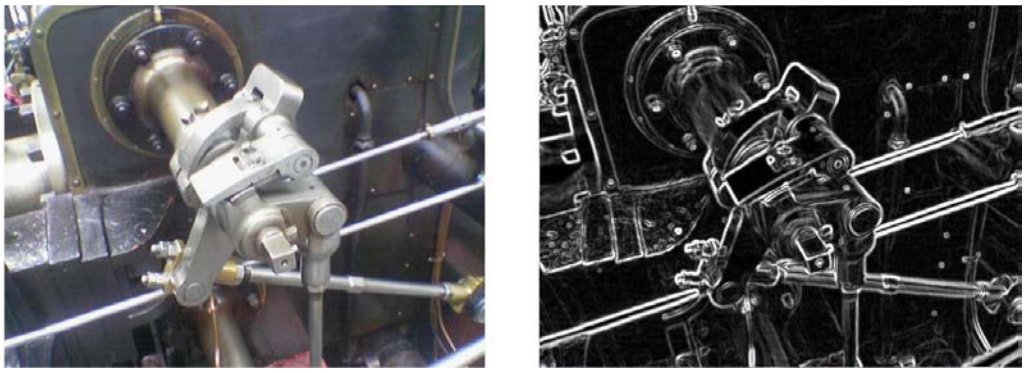

Figure 1-6 A color image and the result of Sobel operator [36].

An alternative of this approach is illustrated in Figure 1-7. In order to enhance the edge detection results, Zhang et al. [37] used a radial search algorithm to extract the lesion from the background. In this method, several radial lines are drawn on the lesion and a radial search for boundary point using the Sobel operator is performed on each line. The points found on individual radial lines are connected using curve fitting algorithms. However, it is found that changing the number of specified lines may alter the final results drastically, adding uncertainty of the accuracy of this approach [38].

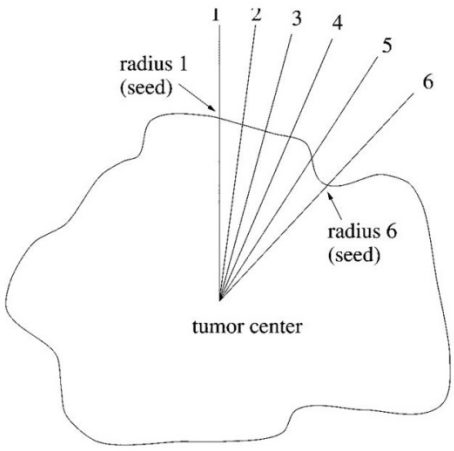

Figure 1-7 A radial search algorithm used for boundary detection [37].

The selected threshold is another subjective factor introduced in those studies, and it may result in wrong border points or the border points cannot be connected to form a closed region [38, 39]. Some other studies also suggest smoothing the border of a mole. Again it is not clear whether those subjective manipulations in defining a mole boundary contribute to any misrepresentation of the actual shape and size of the mole.

Once the border of a mole is determined, the border irregularity can be evaluated based on comparing the mole boundary to that of a regular circular shape. Earlier studies [38, 40] suggest the following expression for evaluating the irregularity index of a 2-D shape:

$$I = \frac{P^2}{4\pi A} \tag{1.2}$$

where P is the perimeter of the shape calculated as the number of pixels along the border of the shape, and A represents the area of the shape and can be calculated by the number of pixels within the shape and on the border of the shape. A simple mathematical calculation can found that the irregularity index is unity for a perfect circle. However, the accuracy of this expression depends on the resolution of the pixel size in the image. It is still needed to develop a method that may be independent of the grid resolutions.

Asymmetry of a shape is typically assessed via comparing pixels on both sides of one of the two principal axes. The two principal axes are determined based on having a product of inertia being zero, and they are passing through the centroid of the shape. It is assumed that the axes are close approximations to the axis of symmetry of the shape. Asymmetry is evaluated via calculating the percentage of the number of pixels that

cannot find their symmetric counterpart pixels to the total number of pixels of that side of the shape. Color variations in a mole have been evaluated via automatic color segmentation based on color information. Other techniques have also been developed to quantify radiance, luminance, and brightness of a mole image. However, those quantities may vary significantly depending on the person who takes the image, and lighting and other adjustments in the environment when the photo is taken [35].

1.5 Other Non-Imaging Processing Products

In November 2011, FDA approved a melanoma detection device developed by a company called MELA Science. The device, *MelaFind*, is a non-invasive tool that provides additional information for dermatologists during the examinations (Figure 1-8). It uses light from visible to near-infrared wavelengths to evaluate skin lesions [41]. It is stated that lights at various wavelengths may penetrate into different tissue depths; therefore, it allows dermatologists to view detailed 3D morphological features of the mole up to 2.5 mm in depth. Hidden cellular patterns in a melanoma leading lesion beneath the skin surface can be viewed and a 3D view is constructed to help dermatologists detect melanomas.

Figure 1-8 The MelaFind detector by MELA science [42].

Another device called Aura is marketed by Verisante Technology to allow rapid scanning of multiple skin lesions on high risk patients. As shown in Figure 1-9, Aura consists of two connecting parts: a handheld probe and a main receiver. The probe is pressed on the skin for a few seconds and the result is shown on the screen of the main unit. Aura utilizes principles of Raman spectroscopy, in which near-infrared laser light changes the vibrational state of the bonds within molecules. The change in vibrational state causes a shift in the light when it is scattered back to the sensor. The magnitude of the shift determines the type and concentration of the molecules in the sample [43].

Figure 1-9 The Verisante Aura, co-invented by Dr. Harvey Lui [43].

The main disadvantages of MelaFind and Aura are their high costs and limited availability. Only professional dermatologists and clinics are able to afford these devices and they cannot be used by the general publics at home; therefore, the patients would still have to go to the doctor's office. It is critical to note that these devices are only meant to help dermatologists analyze lesion structures and/or chemical components and the final diagnoses of melanoma would still need additional medical procedures in a clinical or hospital setting.

1.6 Summary

There are a few smartphone apps available that process images captured by smartphone camera and estimate the risk of melanoma. One app simply uploads images

taken and emails it to a dermatologist nearby for evaluation. Some other apps provide evaluations of the ABCDE system, however, its morphological assessment are labeled as patented technology that cannot be disclosed. Inputs from dermatologists on those software packages suggest low confidence on the accuracy of algorithms assessments. Although image processing is nothing new, based on the review, there is a need to further evaluate different approaches, and develop simple and fast processed algorithms. Since the smartphones are widely available in the market, it is important to develop image processing parameters that are independent of image resolution, lighting, and skills of the photographer.

This thesis research is focused on advancing the image processing techniques and algorithms used for detecting skin melanoma based on photos taken from regular cameras and cellphones. The current methods are limited to basic functions and algorithms that may not provide an accurate assessment, and they are prone to produce false results in many cases. The final product of this research can be used as initial screening method for melanoma, if it is easily accessible to the public. Early stage melanomas are easily curable and they become more fatal as they advance. There is a critical need for a simple and widely available method that prompts visiting dermatologists' office, leading to a reliable diagnosis of melanoma during the early stages.

The long term goal of this study is to develop a smartphone app, which would analyze a photo taken by a phone camera and estimate the probability of melanoma risks based on its morphological features. Since one of the key factors of diagnosing melanoma is tracking how the mole changes during a period of time, the app would compare the image of a particular mole with an older photo of the same mole, stored either on the

device or in the “cloud”. After the app produces initial reports, the images can be sent to several dermatologists nearby to get their feedbacks on the results as well.

To achieve these goals, this thesis is mainly focused on two specific aims:

Aim 1: To develop computational image analyses algorithms to examine skin lesions in the following aspects: asymmetry of the lesion (A), border irregularity (B), color variation (C), diameter (D), and evolving (E), i.e., the ABCDE system. It is expected to extract ratios associated with the severity of the above morphological features of a skin lesion.

Aim 2: To implement the developed MATLAB algorithms to images of benign moles and melanoma leading lesions downloaded from educational and medical websites, as well as provided by dermatologists. It is expected to identify initial cutoff measures associated with the mole asymmetry, border irregularity, and color variation in those images. Quantitative analyses of those images will be performed to evaluate the capacity of the ABCDE to identify ranges of imaging analysis parameters associated with benign moles and melanoma leading lesions, respectively.

The thesis has four chapters. Chapter 1 provides a literature review, limitations of previous research, motivations of the study, and specific aims of the research. Chapter 2 describes the development of the computation algorithms for detecting the mole boundaries, as well as introducing definitions of three ratios (boundary irregularity, asymmetry, and color variation). Implementing the algorithms to mole images downloaded from websites is reported in Chapter 3. We also test whether the algorithm is suitable for providing quantitative assessments to dermatologists on mole images that

have already been identified by dermatologists with visual morphological changes. The last chapter provides the summary of the research and its significance. That chapter concludes with future research directions that can be implemented to improve our understanding of designing better treatment protocols for early detection of melanoma-leading skin lesions.

Chapter 2

Methods and Model Development

This chapter describes the processes of developing normalized (dimensionless) ratios that can be used to assess the ABCDE system of a mole image. It emphasizes the differences between the current and previous approaches. The approaches are illustrated via examples of simplified mole images. It starts with segmentation of a mole image to separate it from its background. Based on the defined mole region with its boundary pixels, the boundary irregularity ratio is defined, followed by step by step derivations of the asymmetry ratio of the mole image, and the color variation ratio.

2.1 Image Segmentation

Currently, cell phones can be easily used to take a picture and to save it as a file readable by the MATLAB® software. A digital photo processes color or grayscale information at all the pixels of the image. In principle, the color or grayscale intensity can be converted into gray scale numbers. In an 8-bit black and white image, 256 (28) different tones can be assigned to each pixel location. A color image is represented by 24 bits, divided into three groups: 8 for red, 8 for green, and 8 for blue. Therefore, a color image may offer 16.7 million (2^{24}) pixel values. The MATLAB® software should be capable of converting a wide variety of imaging file formats (tiff, gif, jpeg, jif, jpx, fpx,

pcd, png, pdf, to name a few) into a matrix containing the pixel locations (coordinates) and tonal values. For example, an image of a chest x-ray may contain *494x600* pixel locations, uniformly distributed on the image, and the resulted matrix may have a function form as, *I(m,n)*, where *I* is the tonal value, and *m* and *n* represent the pixel locations [44].

The first step for analyzing a mole image is separating the lesion from the background. There are various algorithms to detect the edge of the lesion in previous studies. The edge, which typically has the largest change in the intensity and color on the boundary the pixels, can be detected using the first derivative operator as discussed in section 1.4. The change in the tonal value can be assessed by comparing the difference in the successive tonal values along pixels in different directions. Mathematically they are expressed as:

$$I'_x = \frac{\partial \mathrm{I}(\mathrm{x},\mathrm{y})}{\partial \mathrm{x}} \tag{2.1}$$

$$I'_y = \frac{\partial \mathrm{I}(\mathrm{x},\mathrm{y})}{\partial \mathrm{y}} \tag{2.2}$$

Equation (2.1) and Equation (2.2) give the partial differentiations along the *x* and *y* directions, respectively. The calculated partial derivatives will be compared to a prescribed value to determine whether it belongs to the definition of a mole region. This method can detect sharp changes in the tonal values, however, may not be suitable for detecting continual or slow variations in the image [45].

To address the limitation of the first derivative approach, previous studies have proposed to use the second derivative to detect slow changes in intensity, via a Laplace operator,

$$\nabla^2 I(x,y) = (\frac{\partial}{\partial x^2} + \frac{\partial}{\partial y^2}) I(x,y) \tag{2.3}$$

Its finite difference form applied to discrete pixels is given as,

$$\nabla^2 I(i,j) = \frac{I(i+1,j) - 2I(i,j) + I(i-1,j)}{\Delta x^2} + \frac{I(i,j+1) - 2I(i,j) + I(i,j-1)}{\Delta y^2} \tag{2.4}$$

when $\Delta x = \Delta y$, it can be further simplified as:

$$\Delta x^2 \nabla^2 I(i,j) = \left[I(i+1,j) - 2I(i,j) + I(i-1,j)\right] + \left[I(i,j+1) - 2I(i,j) + I(i,j-1)\right] \tag{2.5}$$

Therefore, the above equation will result in a new matrix representing the Laplace operator of the original tonal values.

Figure 2-1 shows the field images of the Laplacian operation of an original tonal file of a mole image. As discussed before, the pixel locations on the boundary of the mole are supposed to have the largest jumps in the Laplacian operation of the tonal field, as they represent the edge of the "light" skin adjacent to the "dark" lesion. In order to pin point the boundary of the lesion, a "threshold" must be defined for the cut off. The pixel locations with a Laplacian operation value larger than the threshold will be counted as the "boundary pixels". The field is then converted into a binary setting with the boundary pixel locations assigned as a value of 1 while the rest have a value of 0.

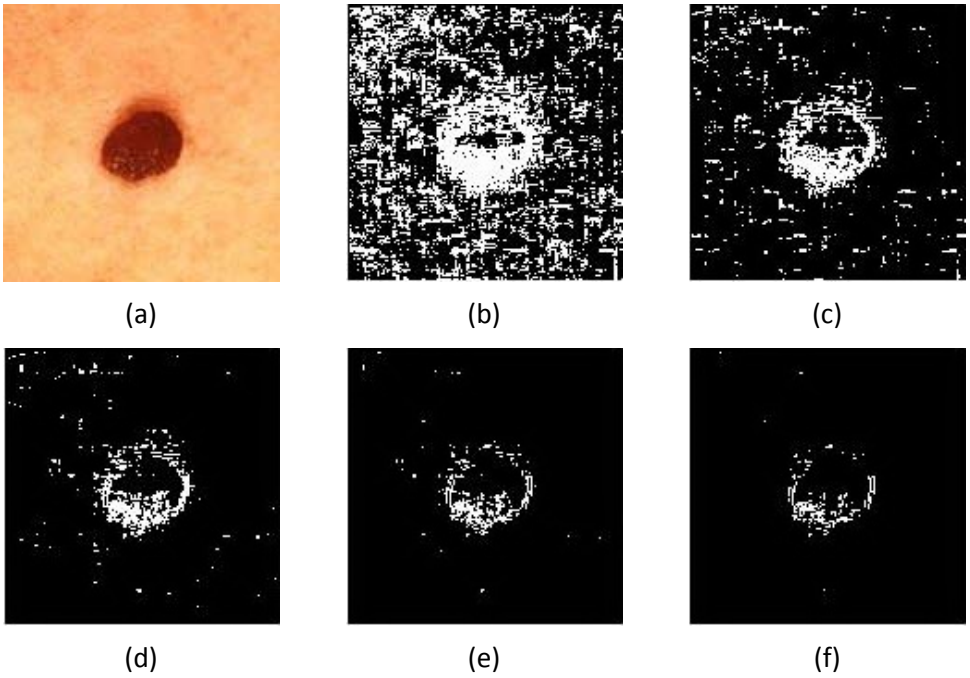

Figure 2-1 Results of boundary detection using derivative method: (a) Original image of the lesion; (b) threshold = 5, (c) threshold =10, (d) threshold = 15, (e) threshold = 20 and (f) threshold = 25.

We have selected a mole image with a very sharp contrast from its background, as shown in Figure 2-1a, Figures 2-1b-f give the generated binary image of the Laplacian field of the tonal values using different values for the threshold. It is disappointing to see that none of the selected thresholds produce a clear delineation of the original mole border.

We have tested the third approach, via delineating the mole border through selection of a cutoff gray scale number of the original tonal field $I(m,n)$. The original color image is converted to a gray scale image with pixel values ranging between 0 and 255. Then a threshold gray scale value is selected to divide the image into two regions: the mole region and the outside background. In Figure 2-2, different gray value cutoff

criteria are applied to the same mole image and the resulting mole edge is illustrated. Figure 2-2c represents the shape of the original mole image very well. Figures 2-2b, 2-2d, 2-2e, and 2-2f exaggerate the irregularities on the top border of the mole, as shown by black circles on individual images. The original mole is erroneously represented in Figures 2-2g and 2-2h. Therefore, by selecting different cutoff criteria, one can identify several processed images with the original mole boundary well represented with high precision. This approach seems better than the tonal derivative methods, in terms of identifying a delineated mole boundary [44].

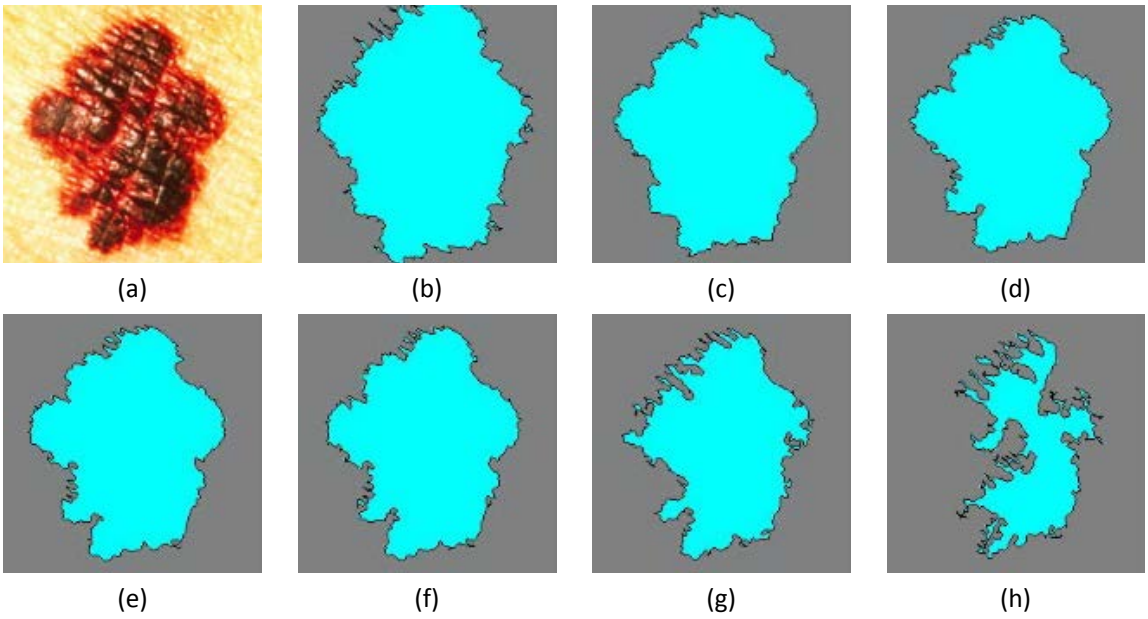

Figure 2-2 Results of boundary detection using binary threshold: (a) the original image, (b) threshold=150, (c) threshold=130, (d) threshold= 110, (e) threshold=100, (f) threshold= 90, (g) threshold= 70, (h) threshold=50.

Figure 2-2 clearly illustrates how subjective the definition of the boundary of an image is when a threshold is chosen. It is important to have an objective method to determine the threshold of the gray scale value to distinguish the mole region from its

background. The method used previously by researchers is based on the Otsu algorithm [46, 47]. This approach is an optimization method to identify a border separating two distinguishingly different clusters of pixels. The optimal threshold gray scale value leads to minimization of an objective function called "the within cluster variance", σ_ω^2, defined by the following equation,

$$\sigma_\omega^2 = W_{mole}\sigma_{mole}^{\ 2} + W_{background}\sigma_{background}^2 \tag{2.6}$$

where $\sigma_{background}^2$ and σ_{mole}^2 represent the background (skin) and the mole variances, respectively. *W* represents the percentage of the pixels occupied within each cluster to the entire image. Therefore, Equation (2.6) can be considered as a weighted average of the variances within an image containing a mole. The Otsu algorithm is demonstrated here using a simple 6*x*6 image shown in Figure 2-3, the same procedure can be applied to images of any size.

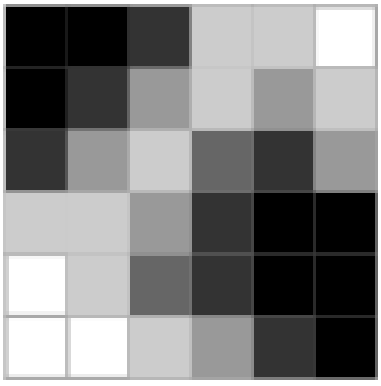

Figure 2-3 A sample 6*x*6 image.

To simplify the calculations, the gray scale intensity range is downscaled from 0-255 to 0-5; 0 being the darkest black and 5 being the white. Figure 2-4 shows the histogram of the sample image based on the assumption made for the gray scale range.

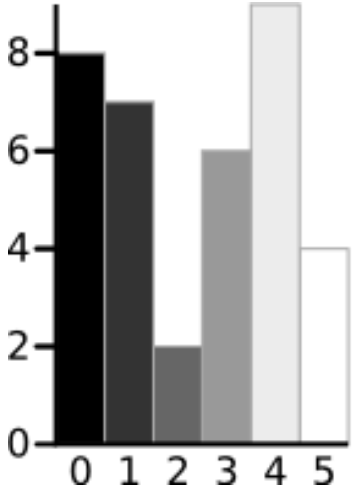

Figure 2-4 Histogram for the sample image.

Figure 2-4 shows that there are 8 pixels having a gray scale value of 0, 7 pixels having a gray scale value of 1, and 4 pixels having a gray scale value of 5 in the image. The following shows how the cluster variance σ_ω^2 is determined if the threshold gray scale value is selected as 3. Any pixels with grayscale values equal to or larger than 3 are considered as in the mole region, while the rest are considered as the background region. The percentages of the two clusters can be calculated using the following equations:

$$W_{background} = \frac{8+7+2}{36} = 47.22\%; \quad W_{mole} = \frac{6+9+4}{36} = 52.78\% \qquad (2.7)$$

The mean value of the gray scale number of each cluster is determined by

$$Mean_{background} = \frac{0x8+1x7+2x2}{8+7+2} = 0.65; \quad Mean_{mole} = \frac{3x6+4x9+5x4}{6+9+4} = 3.89 \qquad (2.8)$$

The variances in individual clusters are calculated similar to calculating a standard deviation and found to be 0.4637 and 0.5152 for the background and the mole, respectively. Therefore, the within cluster variance for a threshold equal to 3 is determined as:

$$\sigma_w^2 = 42.22\% x 0.4637 + 52.78\% x 0.5152 = 0.4677 \qquad (2.9)$$

After selecting any other gray scale value as the threshold, one can determine the within cluster variances, and results are shown in Figure 2-5. It is clearly shown that when the threshold is selected as 3, σ_w^2 is minimized.

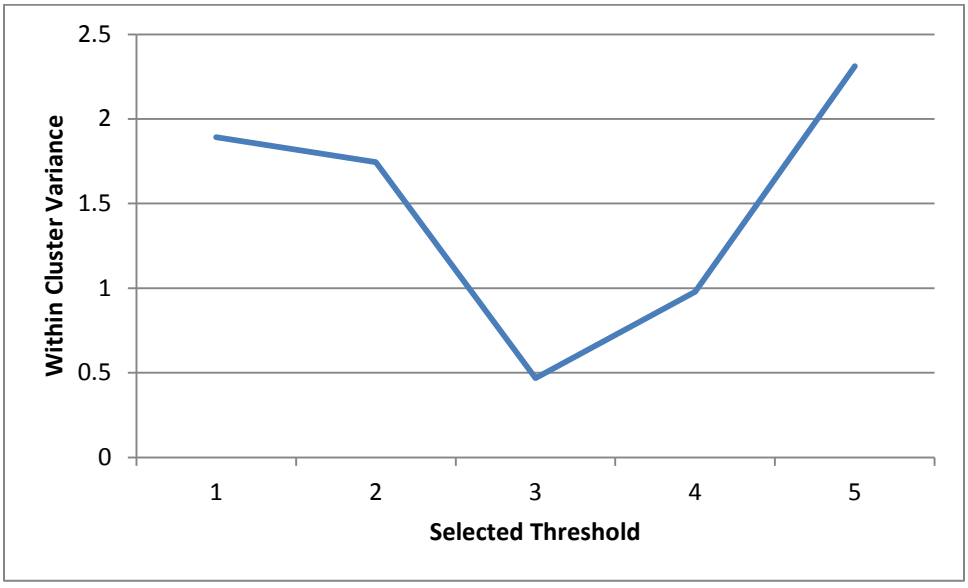

Figure 2-5 Within cluster variance value for different thresholds.

We will apply the Otsu's algorithm to any mole image. A mole image is again converted into a gray scale image with a gray scale value varying from 0 to 255. The threshold gray scale value is selected first as 0 to calculate σ_w^2. The procedures are

repeated 255 times for all the other thresholds. A MATLAB code is written to identify a threshold of the gray scale value leading to minimization of σ_w^2. Figure 2-6 gives the finalized boundary of the mole, when the threshold is determined as 96. It is shown that the identified border of the mole represent very well the shape of the original mole.

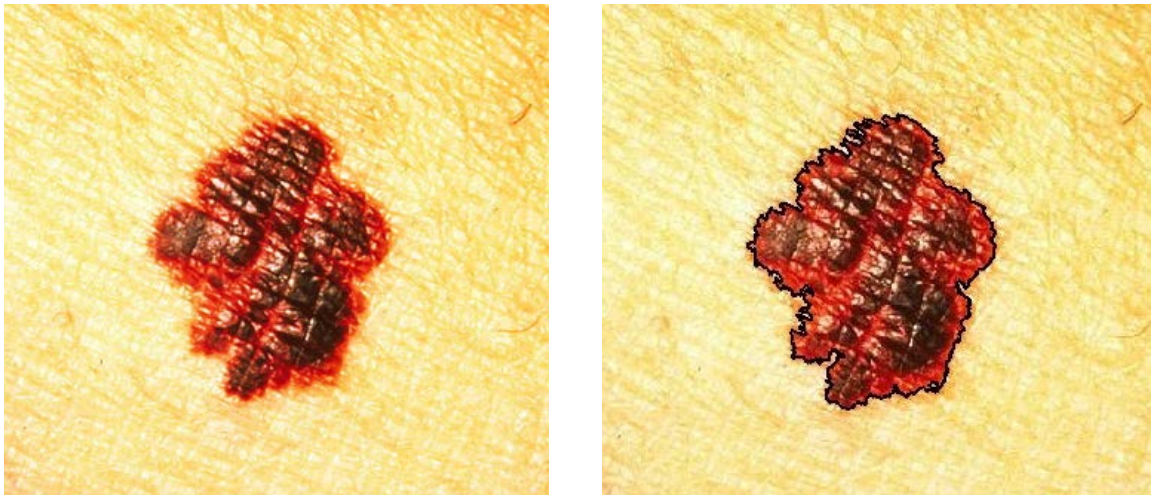

(a) (b)

Figure 2-6 Boundary detection results using the Otsu method: (a) the original image and (b) the detected boundary after minimization of the objective function.

2.2 Boundary Irregularity Ratio

After the boundary is identified and the lesion is extracted from the image, we develop an approach similar to that in Equation (1.1); however, we believe that our approach is less affected by the pixel resolution of the image. Figure 2-7 illustrates how the approach works. Figures 2-7a and 2-7d give the original mole images, while Figures 2-7b and 2-7e show the binary moles with their borders identified. The total number of the pixels within and on the border of the binary mole can be calculated as N_{mole}. Then a perfectly circular shape can be generated with exactly the same total number of pixels, as

shown in Figures 2-7c and 2-7e. In this study, we would compare the border of the mole to that of the circular shape having the same area. The following equation is used to calculate the boundary irregularity ratio, $R_{irregularity}$

$$R_{\text{irregularity}} = \frac{\text{the total number of the boundary pixels of the mole}}{\text{the total number of the boundary pixels of a circle having the same area}} \quad (2.10)$$

A ratio of unity suggests that the shape is perfectly round; however, a ratio larger than one implies that the mole is irregular. Since the calculations of the total number of the boundary pixels are from two images with the same pixel resolution, it is unlikely that the pixel resolution will have a significant effect on the calculation of the boundary irregularity ratio.

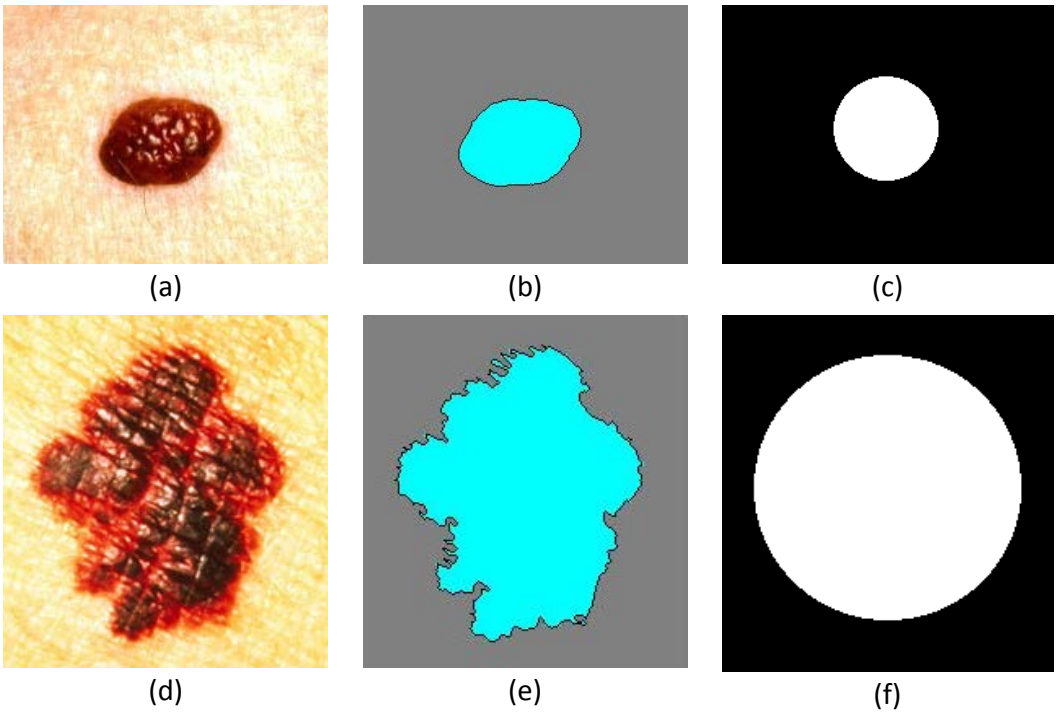

Figure 2-7 The original photos of a regular mole and a melanoma leading lesion (a and d), the detected boundary and extracted lesion from the background (b and e), and the circles with the same area as the mole (c and f).

2.3 Asymmetry Ratio

The general principle of determining the asymmetry of a mole is based on calculating the number of pixels on both sides of the mole not having their mirrored pixels on that other side. Again we would like to develop an objective approach to determine the asymmetry ratio without inducing any subjective interpretation on where the symmetric axis should be. A MATLAB code is written to automatically determine the best symmetric axis, to identify whether the mole image has more than one symmetric axis, and to calculate the asymmetry ratio of the image.

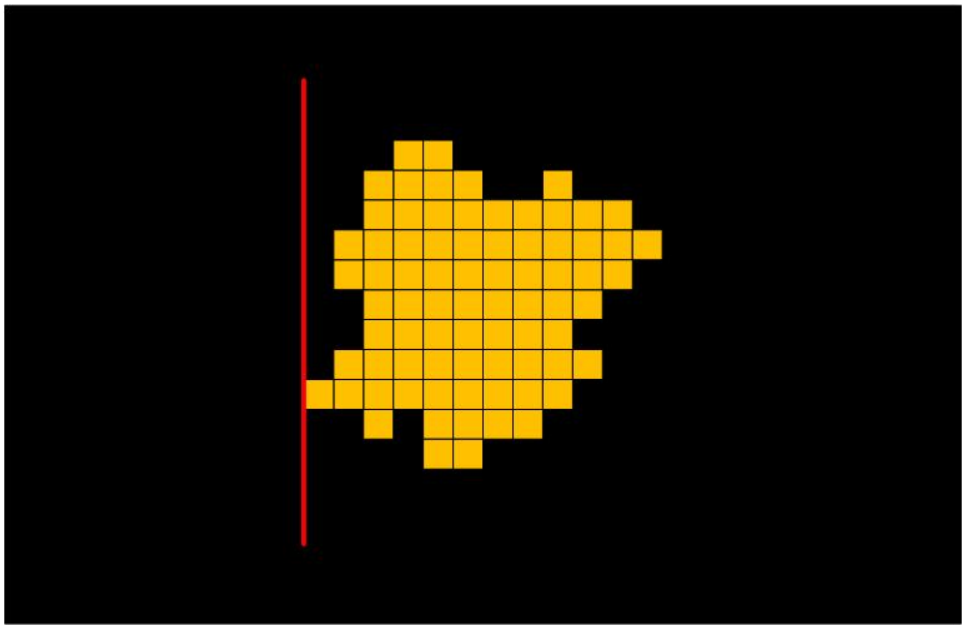

Figure 2-8 A simplified mole image for illustrating the asymmetry ratio calculation.

Figure 2-8 shows a simplified mole identified by the yellow color. The total number of the pixels inside the mole is 77. Assume that the initial orientation of the mole shown in Figure 2-8 as 0°. The symmetric axis (red line in Figure 2-8) is placed at the left edge of the mole region. Therefore, the total number of the pixels that do not have their

mirrored pixels on the other side is also 77. The asymmetry ratio $R_{asymmetry}$ is defined as the ratio of the number of pixels that do not have their mirrored pixels to the total number of pixels inside the mole,

$$R_{\text{asymmetry}} = \frac{\text{total number of pixels having no mirrored counterparts}}{\text{total number of pixels inside the mole}} \tag{2.11}$$

Therefore, $R_{asymmetry}$ in Figure 2-8 is determined as 1 (=77/77).

One can then move the axis line one pixel further to the right side and recalculate $R_{asymmetry}$. Figure 2-9 shows how the symmetric axis affects $R_{asymmetry}$, which decreases to 75/77 or 67/77, when the symmetric axis is located one or two pixels from the left edge of the mole, respectively. When the symmetric axis is located six pixels from the left edge, $R_{asymmetry}$ reaches its lowest value of 15/77. It then increases when the symmetric axis continues to move to the right. Therefore, for the orientation of 0°, $R_{asymmetry}$ is determined as 0.195 (15/77).

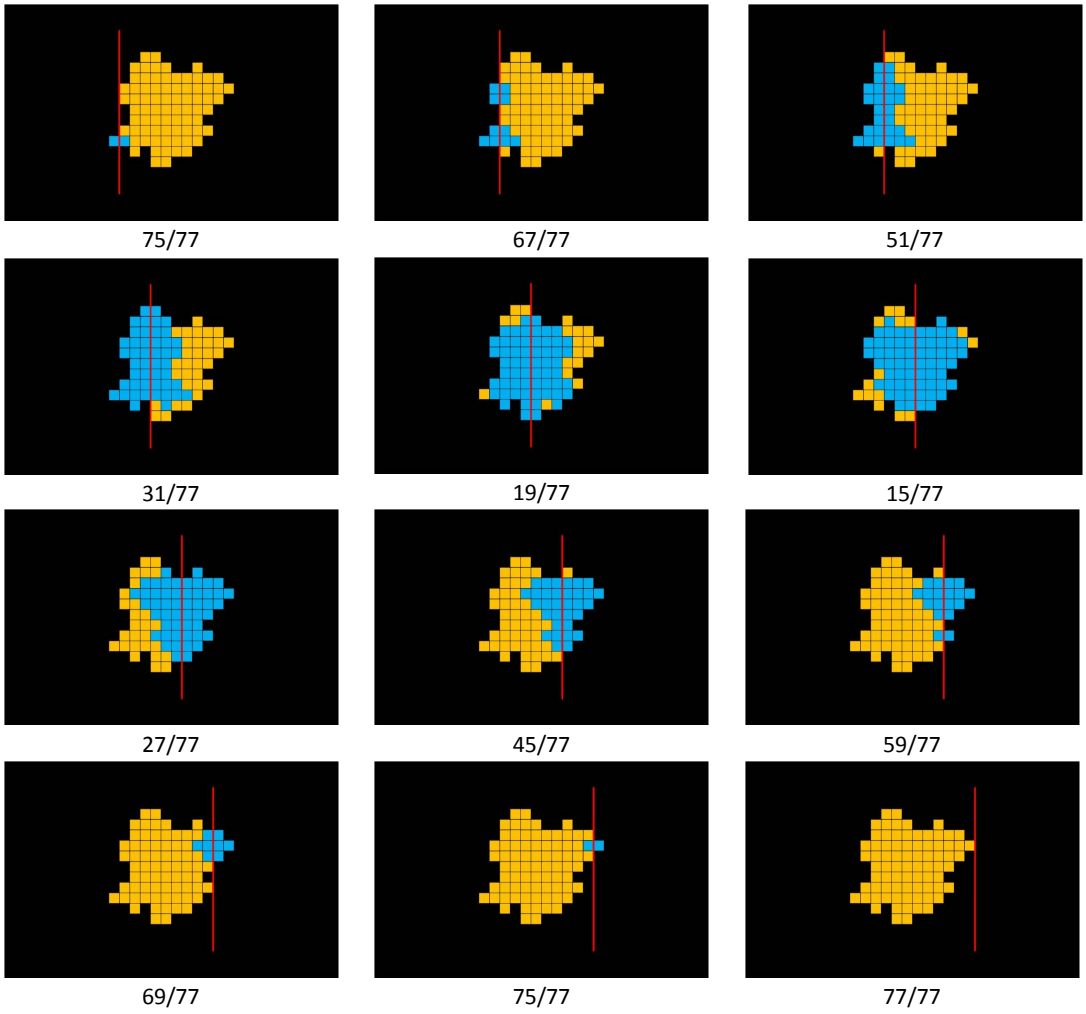

Figure 2-9 Demonstration of the basis of symmetry analysis algorithm

The mole image is then rotated by 10°, and the MATLAB codes are re-run to determine the lowest $R_{asymmetry}$ for the 10° orientation. The above procedures are repeated 18 times to cover the rotation of the image from 0° to 170°. Figure 2-10 illustrates how the asymmetry ratio is calculated when the orientation is at 90° for the same mole shown in Figure 2-8

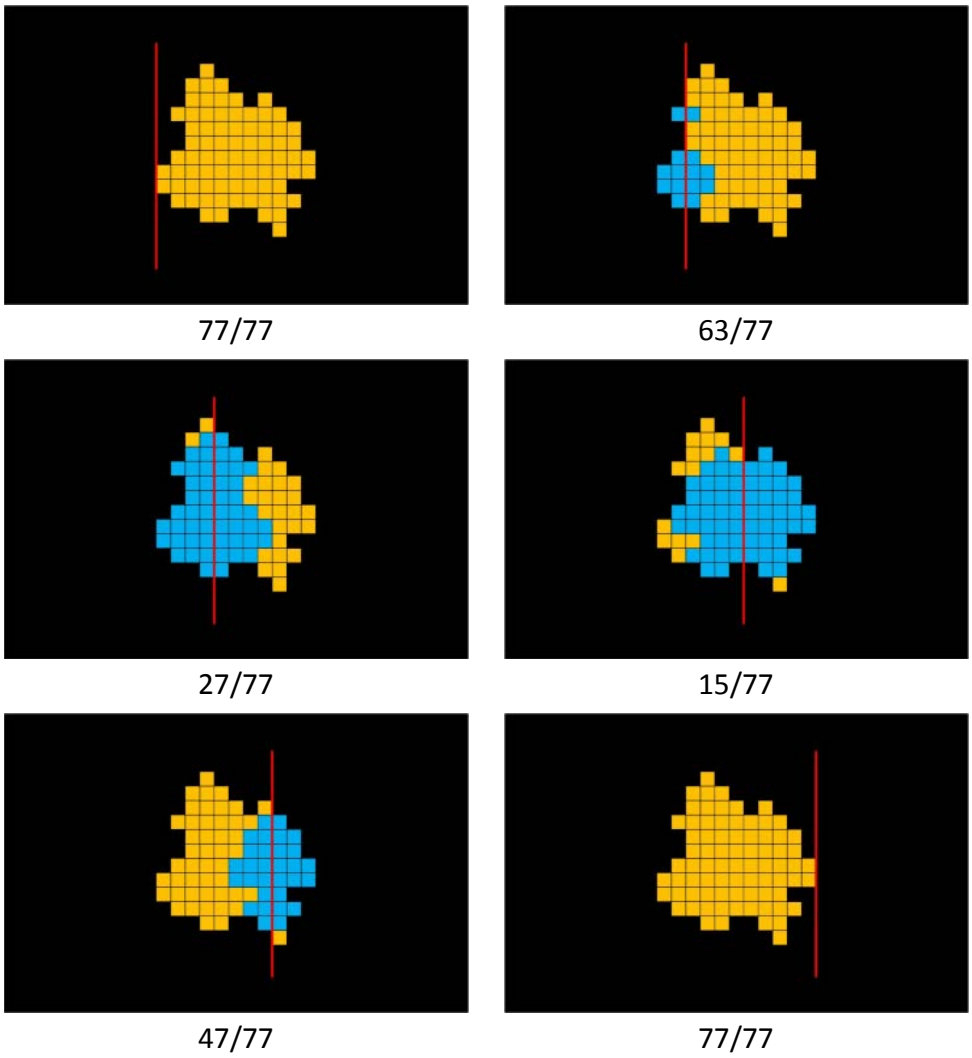

Figure 2-10 Symmetry analysis algorithm on the 90° rotated image.

The approaches are implemented to a mole image shown in Figure 2-11. $R_{asymmetry}$ is calculated for all 18 orientations (0° to 170°, at an increment of 10°). The results are plotted in Figure 2-12. The maximal value of the $R_{asymmetry}$ (0.47) is identified when the orientation is at 160°, followed closely by 0.46 at 70°. The lowest $R_{asymmetry}$ occurs at 30° as 0.12, although $R_{asymmetry}$ at 120° (0.14) is slightly large than that.

Figure 2-11 A sample lesion for symmetry analysis.

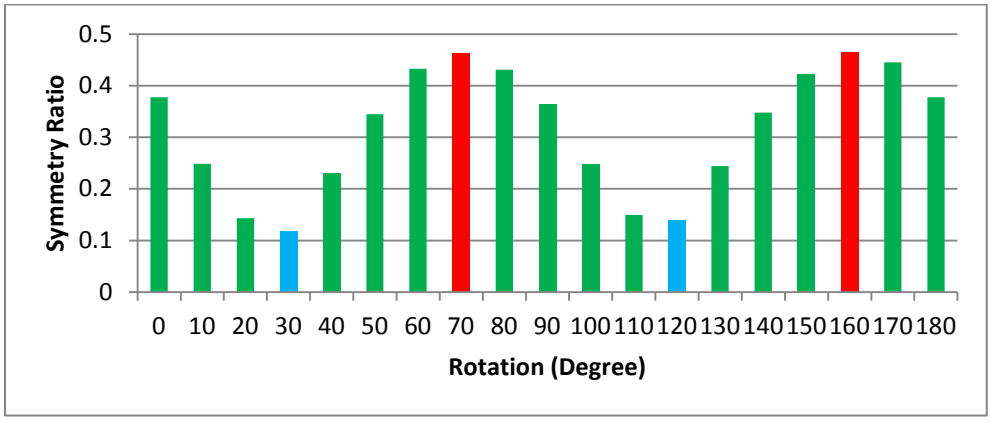

Figure 2-12 Symmetry ratios for 10 degree interval rotations.

Two axes are placed on the original mole image in Figure 2-13 to illustrate the symmetrical feature of the mole image when the axes are placed at 30° or 120°. For this image, $R_{asymmetry}$ is determined as 0.12 or 12%, identified by the MATLAB code at the orientation of 30°. In another word, once the symmetric axis is selected at the 30° orientation, 12% of the pixels do not have their symmetric counter pixels.

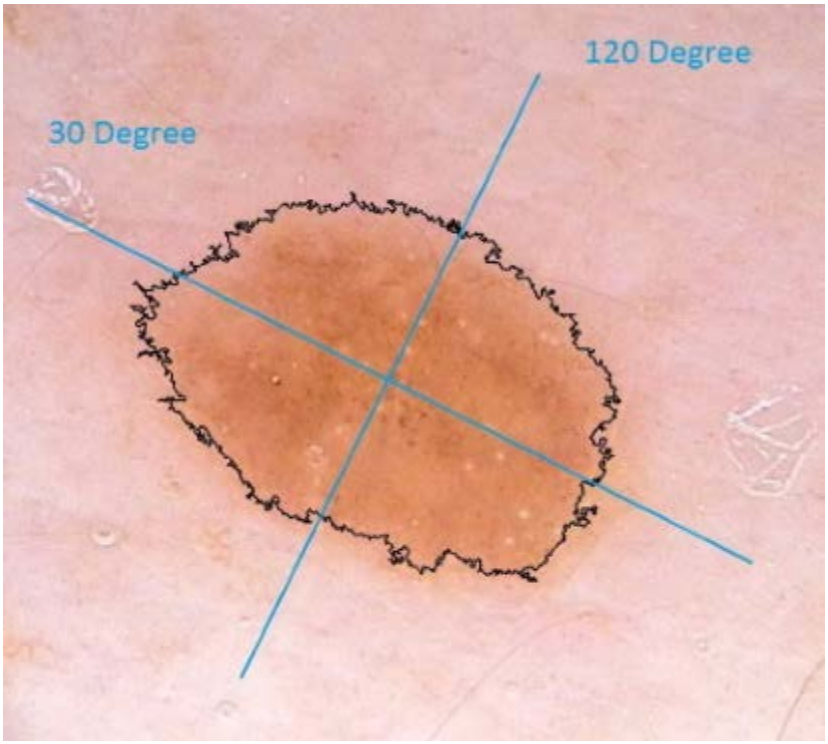

Figure 2-13 Symmetry axes determined for the sample image.

2.4 Color Variation Ratio

After a mole region is identified, one can assess the color variation inside the mole. We have tested whether using a color histogram is appropriate for the assessment. If the mole has a uniform color or gray scale value, the histogram should give one peak, while if the mole is patched with two or three distinguished colors, two or three peaks occur in the histogram. However, our preliminary analyses have demonstrated that the histogram could not produce narrow peaks as expected. In this study we develop a simple method to quantify color variation within a mole [48, 49].

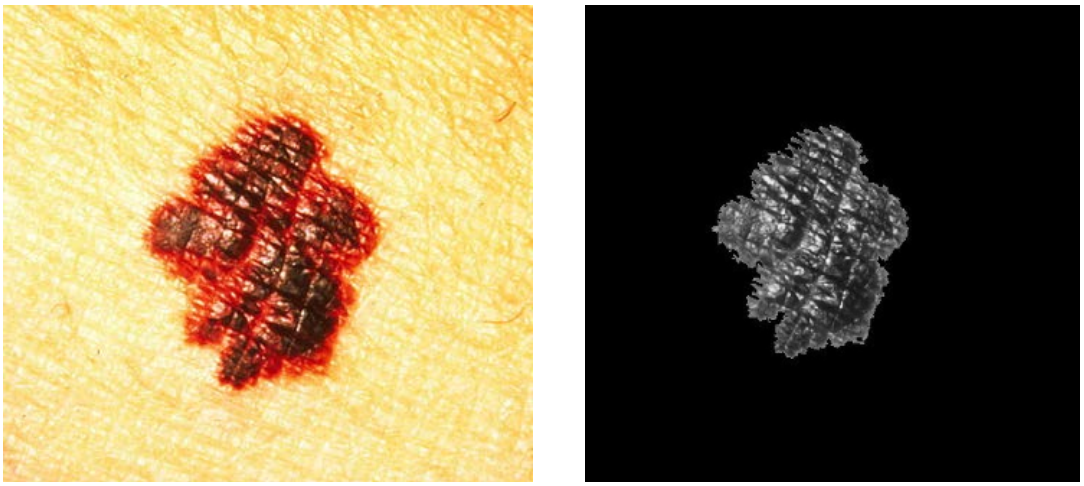

(a) (b)

Figure 2-14 (a) The original image and (b) the image converted to grayscale.

The first step is to identify the boundary of the mole as described previously. Rather than changing the mole image to its binary form, the original gray scale values of individual pixels insides the mole are retained. Figure 2-14 shows the original color image of the mole and the gray scale image of the mole. The next step is to calculate the average gray scale number of all the pixels inside the mole. Then, the standard deviation of the gray scale numbers of all the pixels can be determined. The color variation ratio is defined as:

$$R_{\text{color variation}} = \frac{\text{standard deviation of the pixel gray scale values}}{\text{mean value of the pixel gray scale values}} \tag{2.12}$$

Again, since the ratio is calculated based on the same image, the image pixel resolution and lighting of the background will unlikely affect the color variation ratio.

2.5 Mole Diameter and Evolution with Time

The size of a mole can be assessed using the diameter of an equivalent circular shape having the same area. Once a ruler is placed with the mole when the image is taken, the pixel size can be determined to then identify the size of the mole. The mole size is an important morphological feature of the mole since it can be used to evaluate how the mole evolved with time. It is much easier to evaluate mole evolution if the image is taken over time, preferably under the same photographic conditions.

Chapter 3

Results

This chapter includes the results of implementing the developed MATLAB codes to various lesion images to assess their morphological features. The images used can be categorized into two groups:

1. Benign mole and melanoma leading lesion images downloaded from several websites.

2. Lesion images provided by a dermatologist.

In this chapter, we first display all the lesion images from both groups. The result of segmentations using the MATLAB codes is provided. To verify the Otsu method of segmentation, all the "within cluster variance" values for a random image are calculated and the boundary produced by the minimum variance value is shown. Using the boundary obtained from the segmentation, the pixels inside and on the boundary are counted and the boundary irregularity ratio ($R_{irregularity}$) is calculated. Finally, the asymmetry and color variation ratios are calculated using the method demonstrated in sections 2.3 and 2.4. Since the mole images downloaded from websites have been labeled either "benign" or "melanoma leading", a cutoff ratio is identified with a percentage of statistical confidence. For the mole images provided by the dermatologist, we only illustrate whether the calculated changes of the ratios over time are consistent with the impressions of the changes by the dermatologist. Information on whether those moles are melanoma

leading is unavailable at this time. The experimental procedures involving human subjects have been reviewed by the IRB at UMBC and were approved.

3.1 Lesion Images

Several medical websites were searched to obtain two groups of benign and melanoma leading lesion images. Ten images in each group that had a high image resolution and acceptable quality were chosen for further analyses. Figure 3-1 shows the benign mole images. The melanoma leading lesions that were selected are shown in Figure 3-2. The first visual impression of the benign mole images is their roundness, uniform color, regular borders, while the melanoma leading lesions are rugged, patched, and asymmetric in shape.

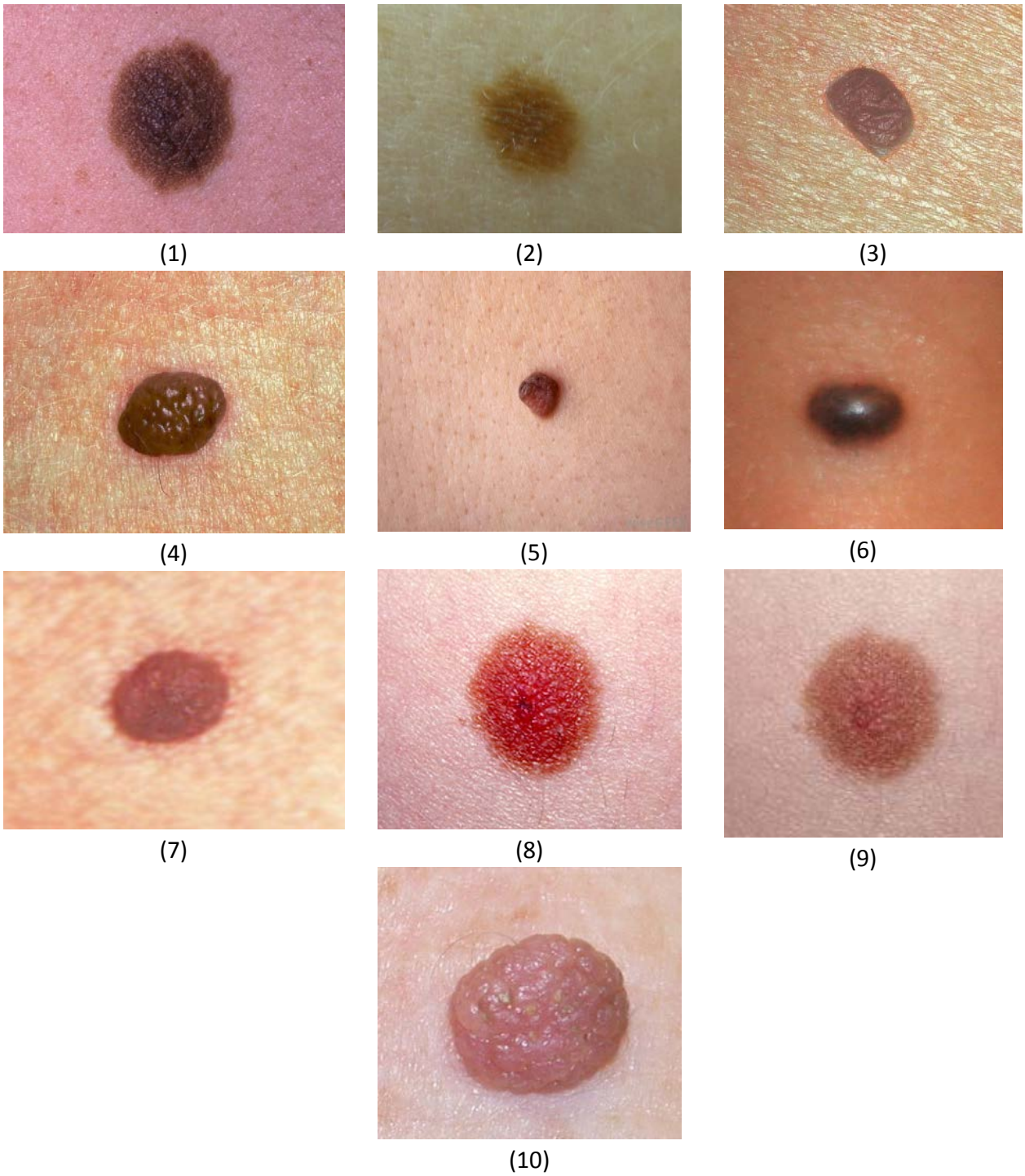

Figure 3-1 Ten benign lesion images downloaded from various websites.

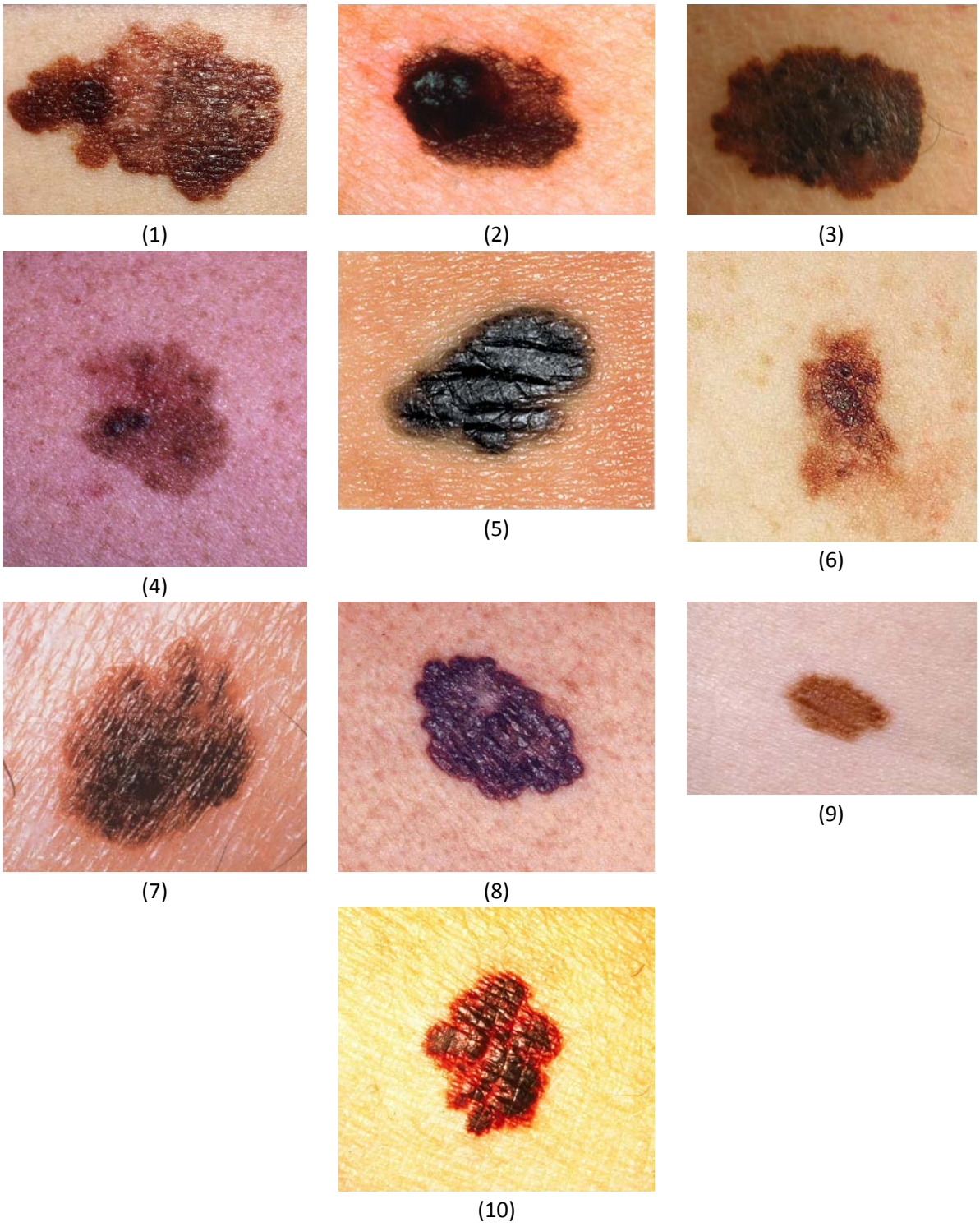

Figure 3-2 Ten melanoma leading lesion images downloaded from various websites.

The second group of mole images from real patients is provided by a dermatologist. As one may see, all images look like having irregular shapes. For each mole, two images are obtained, one is the initial photo of the image, and the other is the photo of the same image taken 6 or 12 months later. Figures 3-3 and 3-4 show the initial set and the final set of the images, respectively. According to the dermatologist's professional observation, the mole lesions in this group have changed after the period of time.

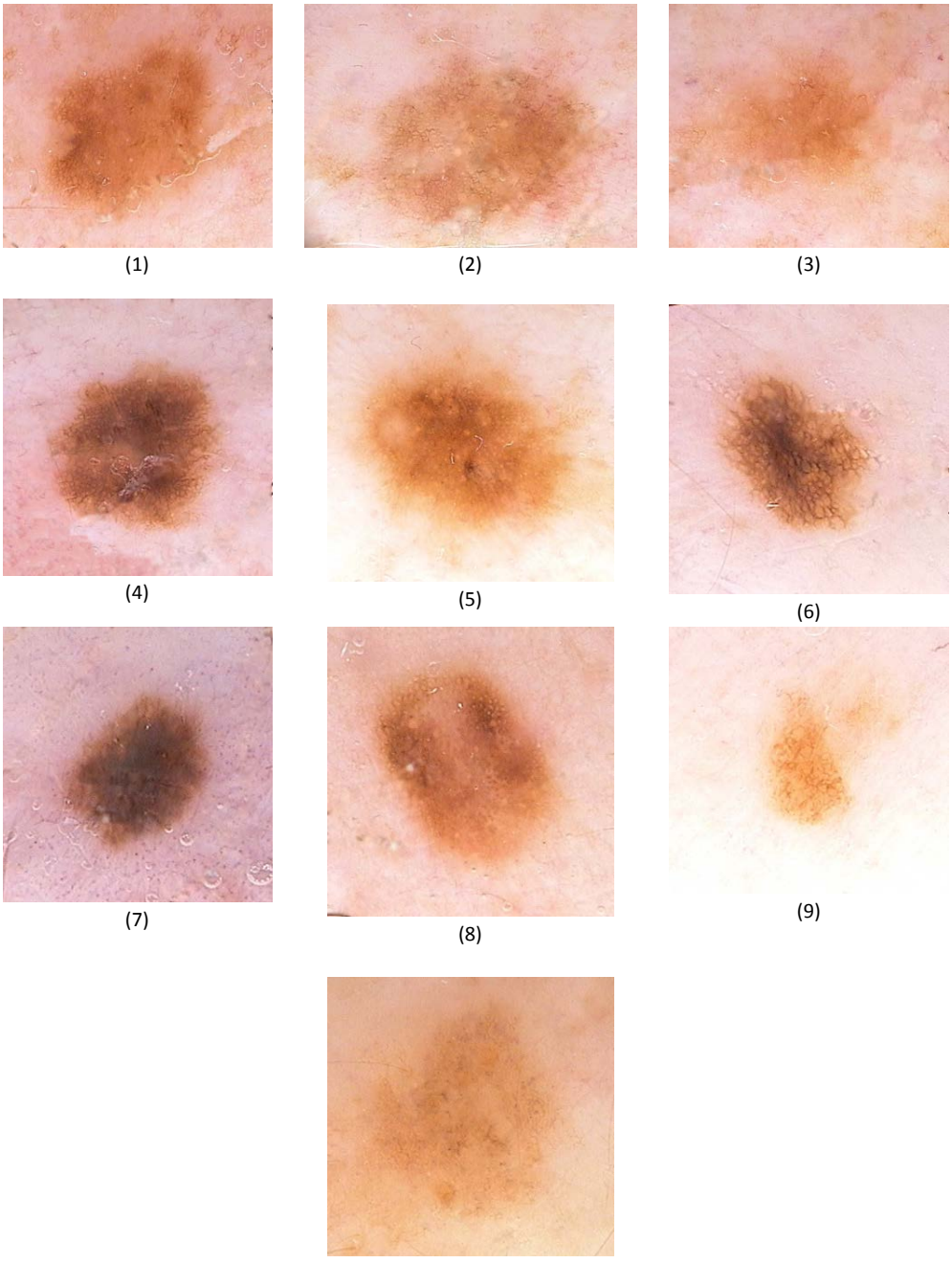

Figure 3-3 The initial set of the mole lesions provided by the dermatologist.

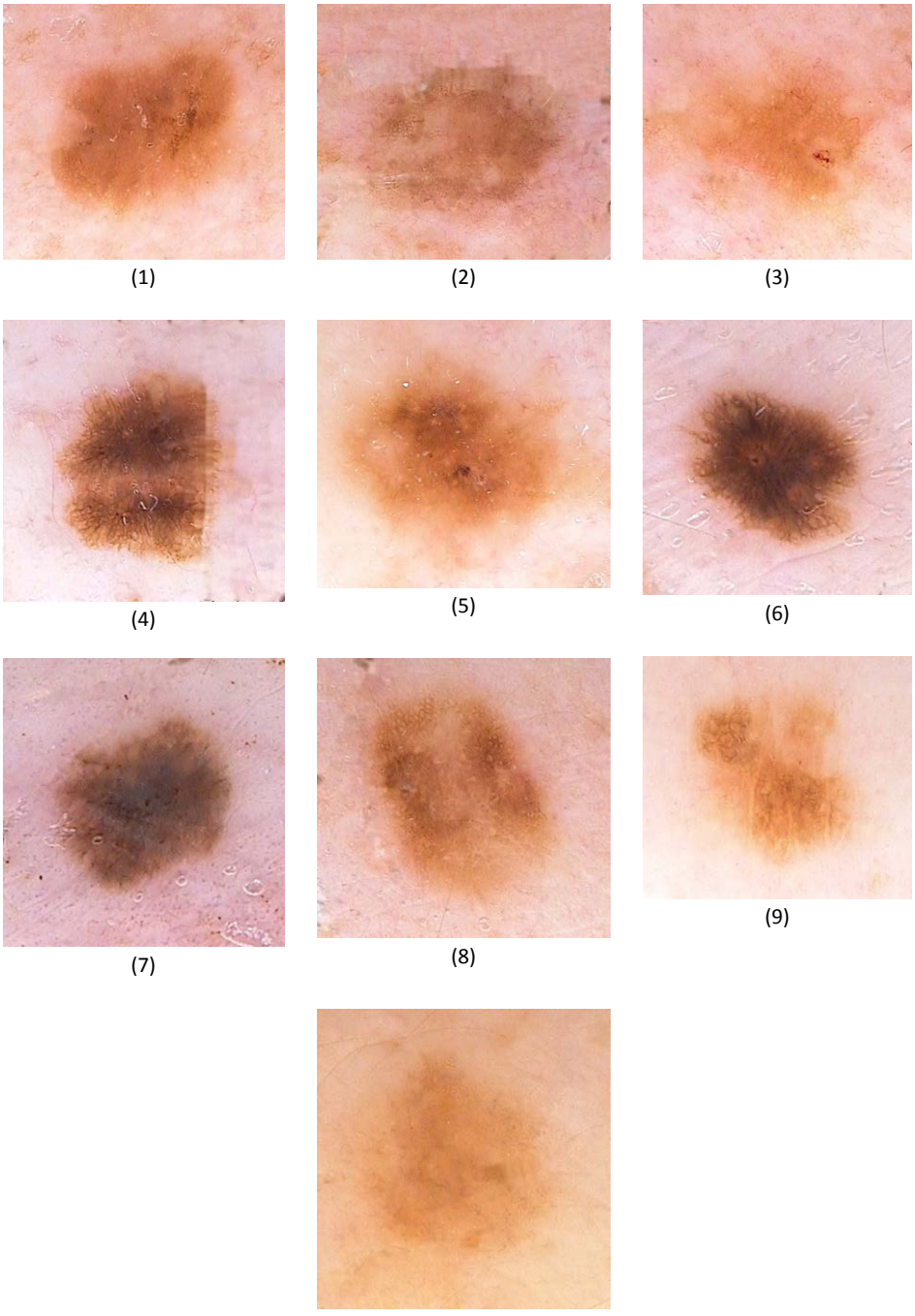

Figure 3-4 The final set of the mole lesions provided by the dermatologist.

3.2 Segmentation

Firstly, the segmentation algorithm is run on the input image to separate the lesion from the background skin. As discussed in section 2.1, various threshold values are selected and the "within cluster variance" is calculated for each selection. The number that produces the minimum variance is chosen as the segmentation threshold value. Figure 3-5 demonstrates the boundary line produced by different threshold values ranging from 58 to 182. The minimal variance is then calculated for each selected threshold value of the grayscale number. As shown in Figure 3-6, the minimum variance occurs when one chooses the grayscale number of 132 as the threshold.

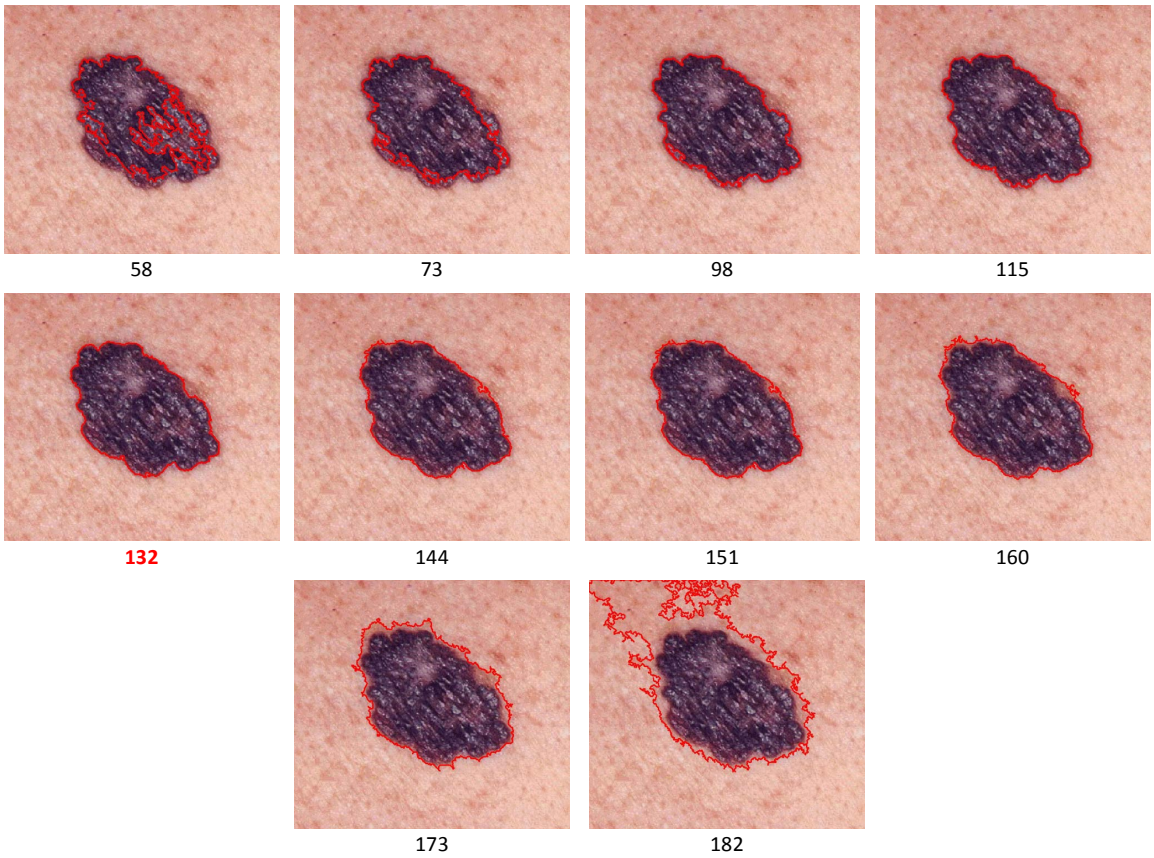

Figure 3-5 Various boundary detection results of a single lesion image when one selects different pixel values as the threshold. The red line delineates the boundary of the mole.

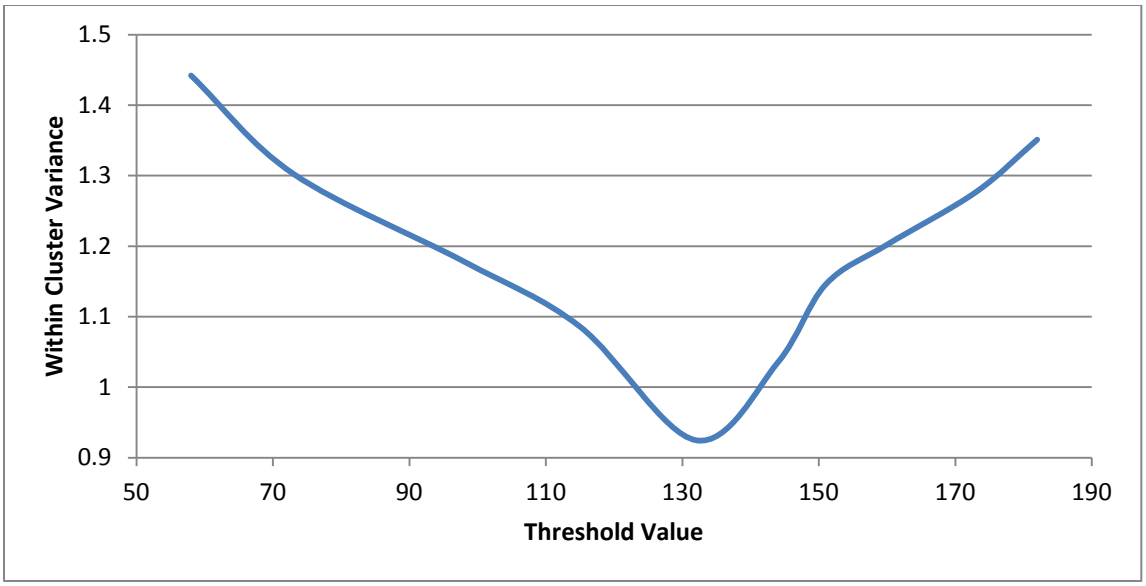

Figure 3-6 The within cluster variances (σ_w^2) as a function of the threshold value of the grayscale number.

Using this algorithm, all the sample images are segmented and the lesion boundaries are detected. Figure 3-7 shows the boundary detection results on a random melanoma leading lesion and a benign mole. Note that the delineated mole border agrees well with that in the original mole image.

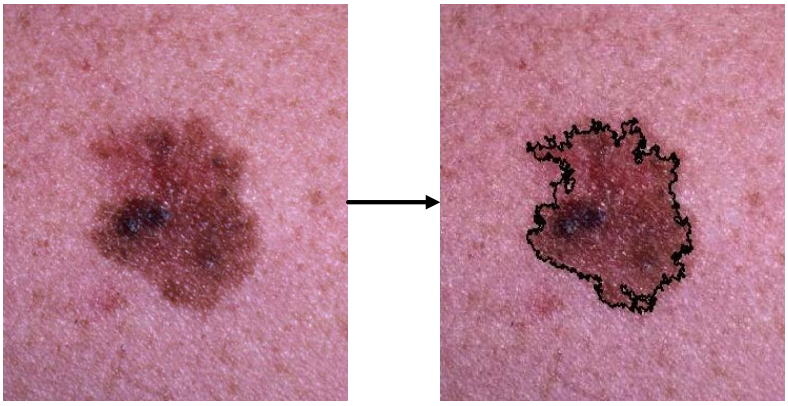

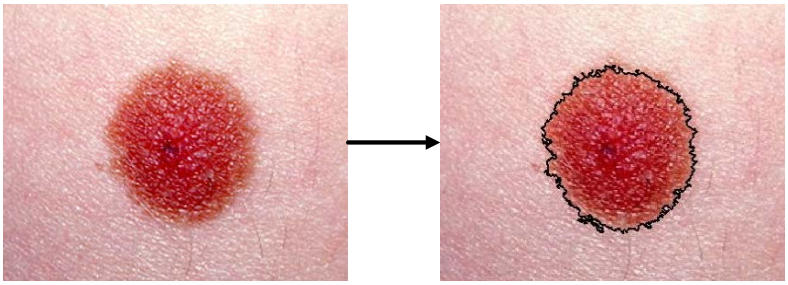

Figure 3-7 The boundary segmentation results for a melanoma leading and a benign mole.

3.3 Irregularity Ratio

The detected boundary in the previous section is used to calculate the irregularity ratio. In order to calculate this ratio, the code runs the following steps:

1. The pixels on the boundary (the black pixels in Figure 3-7) and the area pixels representing the perimeter and the pixels inside the boundary, respectively, are counted.
2. A circle with the same area is drawn and the number of pixels on its boundary is determined.
3. The irregularity ratio is calculated using Equation (2.10).

Shown in Figure 3-8a, a mole lesion is extracted from its background. In Figure 3-8b, a circle with the same area as that in Figure 3-8a is illustrated using the MATLAB codes. Since our drawing platform is the computer screen and pixels which are used to draw images and shapes are "discrete" units, it is not always possible to draw a circle that has the exact area obtained from the original image. When that happens, interpolation is used based on results of two circles with a radius difference by one pixel size.

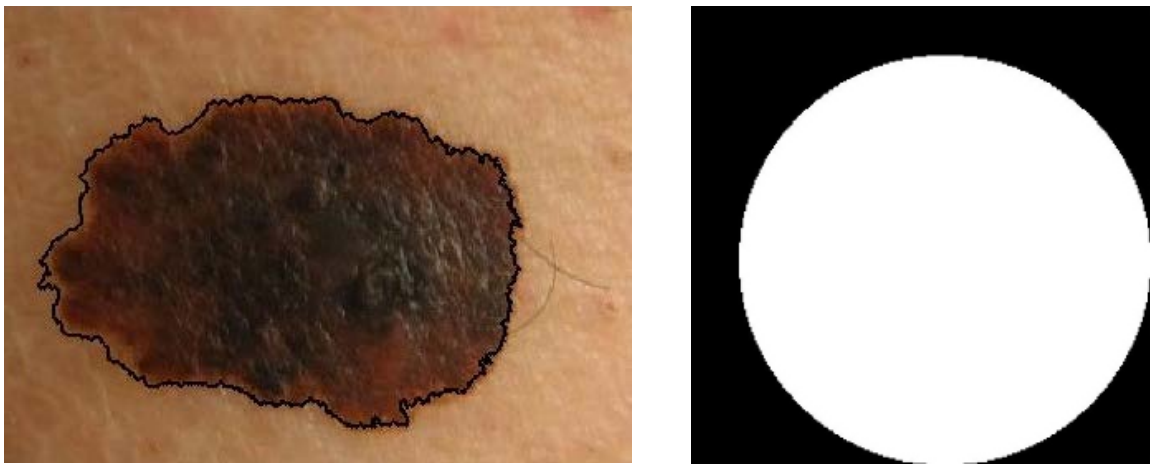

(a) (b)

Figure 3-8 (a) A melanoma leading lesion with its detected boundary, and its calculated area and perimeter calculated, and (b) a circle drawn with the same area as the lesion.

The original lesion in Figure 3-8a has 25,835 area pixels and 1385 boundary pixels. Then the calculated boundary pixels of a circle with the same area pixels as the original lesion are found to be 570. The boundary irregularity ratio is then calculated as

$$R_{\text{Irregularity}} = \frac{\text{Lesion Perimeter}}{\text{Equivalent Circle Perimeter}} = \frac{1385}{570} = 2.4314 \qquad (3.1)$$

Using the same algorithm, one calculates the normalized irregularity ratios for all the 20 melanoma leading and benign mole samples and they are listed in Table 3-1. Note that the sample number is random. The average irregularity ratio in the benign mole group is 1.63, while it increases to 2.38 in the melanoma group. The variations of the irregularity ratios in each group are represented by the standard deviation (SD in Table 3-1). The results are plotted in Figure 3-9. This figure also illustrates the mean value of each group. As shown in Figure 3-9, the cutoff irregularity ratio is 1.96 when the Mean ± 0.89SD ranges of both groups do not overlap each other. When the irregularity ratio is bigger than 1.96, one can state that it is a melanoma leading, while it is a benign mole when the ratio is smaller than 1.96. If one assumes that the distribution in each group is Gaussian, one may calculate the confidence of classifying a mole into its distinguished group as 63.19%, due to the ±0.89SD shown in Figure 3-9. In another word, when the cutoff is selected as 1.96, 63.19% of time the mole will be grouped correctly.

Table 3-1 Normalized irregularity ratio results for melanoma leading and benign mole images downloaded from various websites.

Sample No.	Melanoma	Benign Mole
1	2.8647	1.9523
2	1.7716	1.6699
3	2.4314	1.8645
4	2.4782	1.1863
5	2.0325	1.5505
6	2.6201	1.1834
7	3.1621	1.0856
8	1.8275	2.075
9	1.8052	1.6306
10	2.8001	2.1482
Mean	**2.38**	**1.63**
STD	**0.47**	**0.36**

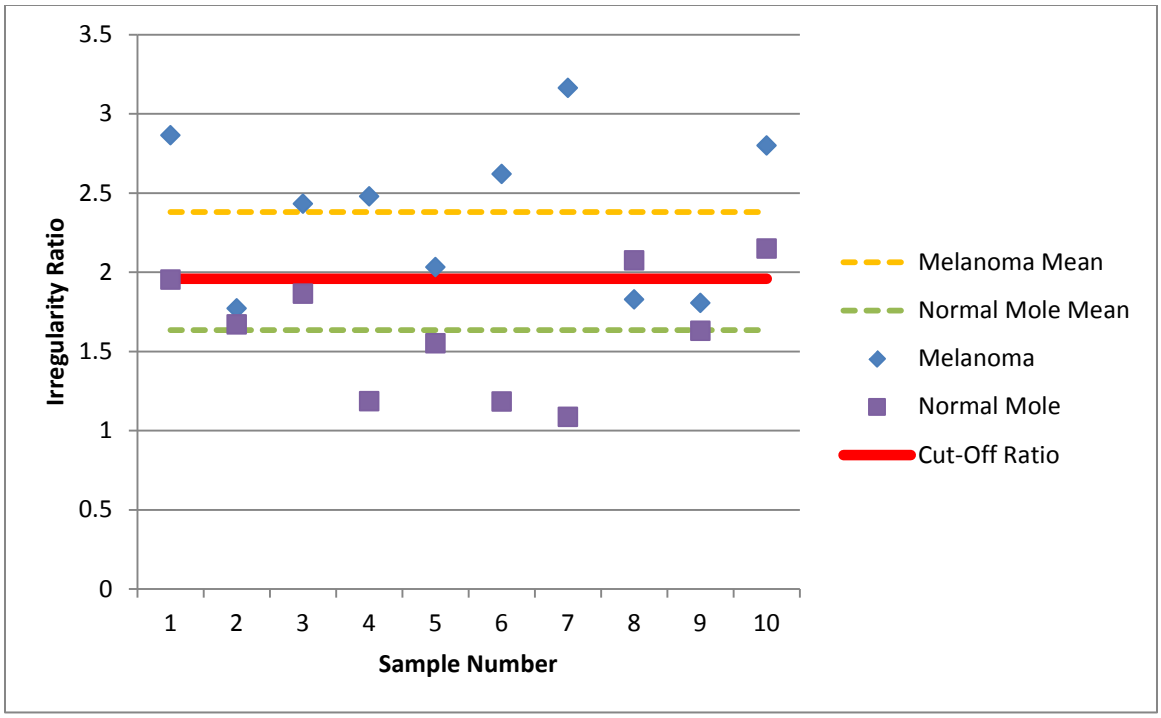

Figure 3-9 Comparison of the melanoma leading and bengin mole irregularity ratios of the 20 mole images downloaded from various websites. The identified cutoff ratio to classify one mole images to its group is represented by the solid line.

3.4 Asymmetry Ratio

Following the algorithm discussed in section 2.3, one can see a 20° rotation of the original sample (Figure 3-10a) in Figure 3-10b, and the identification of the best symmetric line drawn in Figure 3-10c. The total pixel number of the entire mole is 5940. About the symmetric line in Figure 3-10c, the number of the pixels that do not have their symmetric counter pixels is 699. The asymmetric ratio is then calculated as

$$R_{\text{Asymmetry}} = \frac{\text{Number of pixels w/o its counter pixels}}{\text{Total number of pixels of the lesion area}} = \frac{699}{5940} = 0.1176 = 11.76\% \quad (3.2)$$

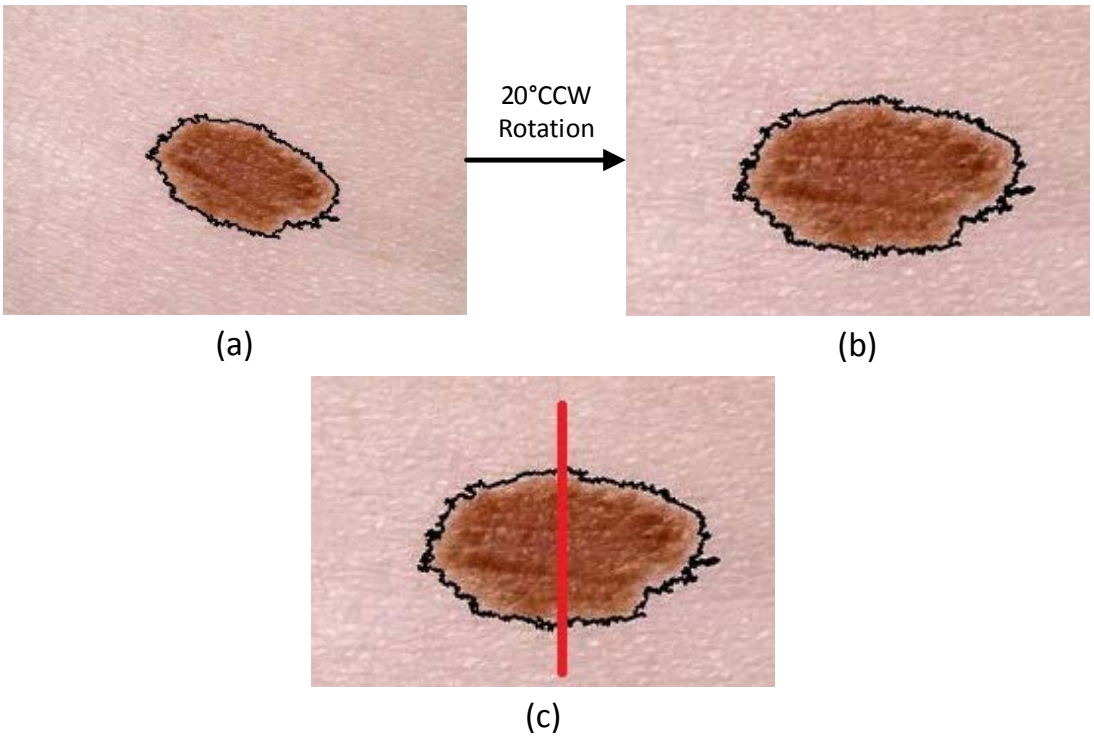

Figure 3-10 (a) A melanoma leading sample, (b) the sample rotating 20° counter-clockwise from the original orientation (c) the rotated sample with tis symmetry line.

Using the same algorithm, the normalized asymmetry ratios of all 20 melanoma leading and benign mole samples are calculated and listed in Table 3-2. The mean value of the asymmetric ratios in the benign mole group is 0.083, implying 8.3% of the pixels having no symmetric counter pixels. The mean value of the asymmetric ratios in the melanoma group increases by 98% to 0.164, or a degree of 16.4% asymmetry. Figure 3-11 shows the results obtained from the two groups, with their non-overlapping statistical ranges. Following the same statistical analyses, one can identify a cutoff asymmetric ratio as 0.109 to distinguish a benign mole from a melanoma leading. If one assumes a Gaussian distribution in the samples, the confidence for grouping a mole image correctly to its group is 81%.

Table 3-2 Asymmetry ratios of the melanoma leading and benign mole samples.

Sample No.	Melanoma	Benign Mole
1	0.20623	0.089887
2	0.13627	0.092048
3	0.12185	0.10647
4	0.23587	0.080286
5	0.16345	0.12081
6	0.22135	0.072323
7	0.12867	0.063524
8	0.12065	0.086338
9	0.11768	0.072839
10	0.19174	0.044808
Mean	**0.164**	**0.083**
STD	**0.043**	**0.020**

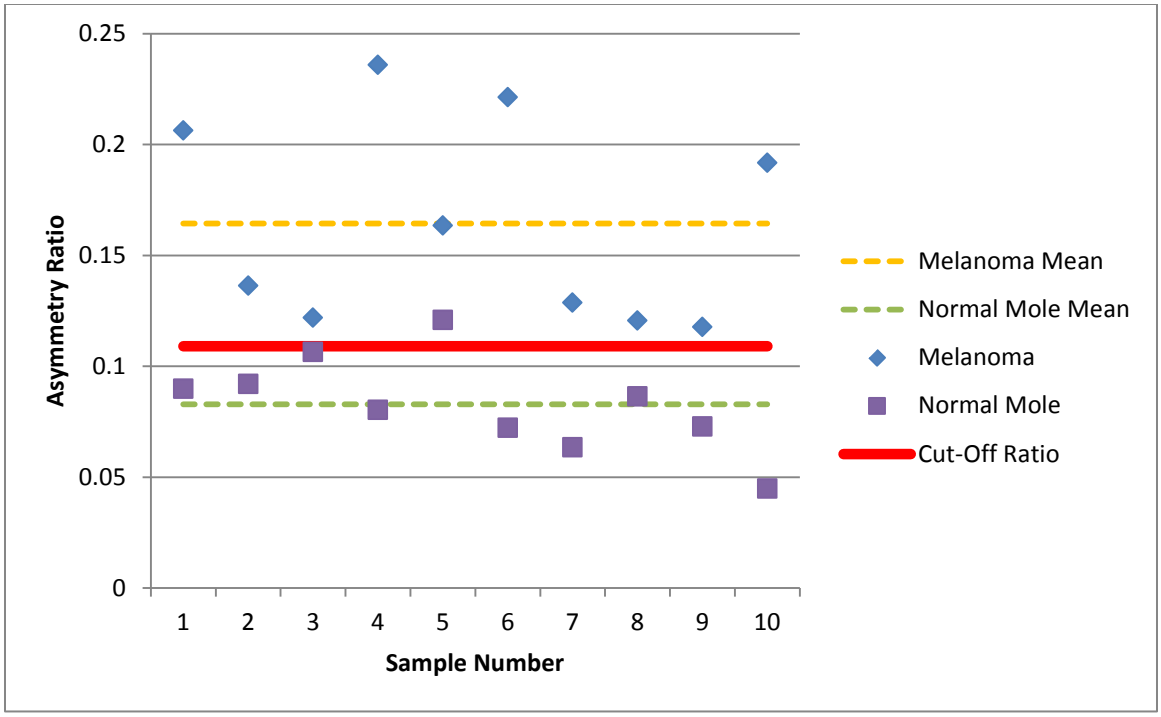

Figure 3-11 Comparison of the asymmetric ratios for the melanoma leading and benign moles.

3.5 Color Variation Ratio

The lesion color variation ratio is obtained via first converting the image into its grayscale image, showing in Figure 3-12. The benign mole appears more uniform in grayscale variations, while the melanoma image consists of pixels with a wider range of grayscale values. The calculated color variation ratio of the benign mole in Figure 3-12a is 0.09, implying a relatively uniform grayscale values within the mole. On the other hand, the mean±SD for the melanoma leading is 78.87±58.87, and the color variation ratio in the melanoma leading in Figure 3-12c is then calculated as 0.68.

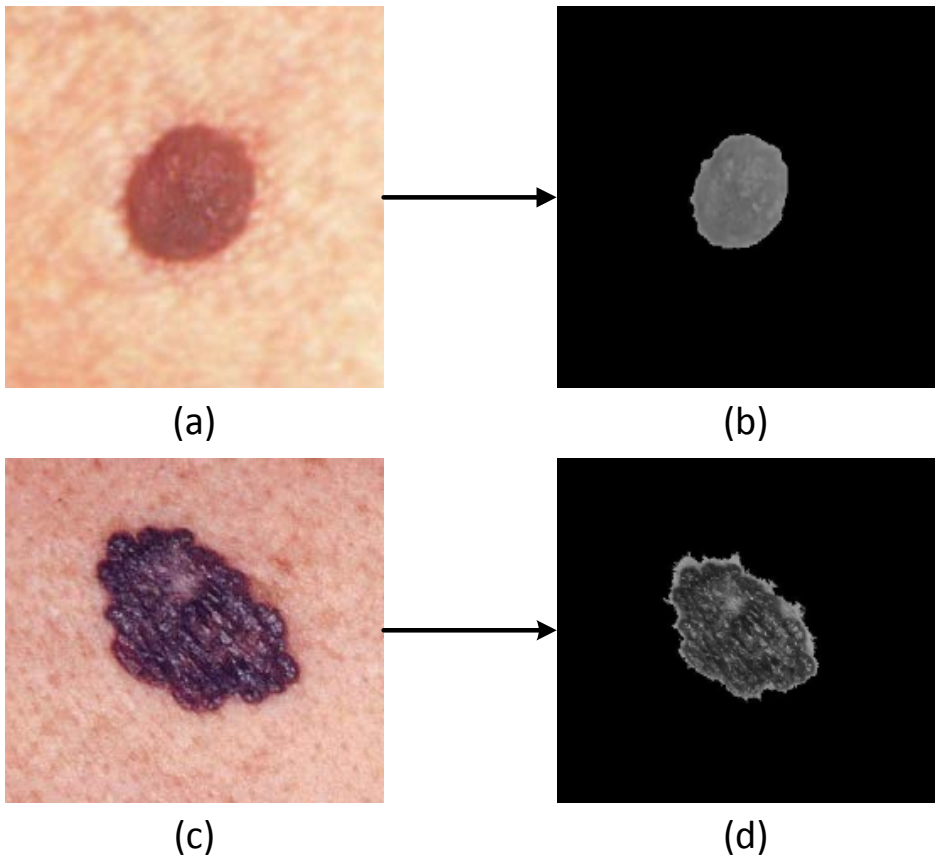

Figure 3-12 (a) A benign mole sample, (b) the grayscale image of benign mole, (c) a melanoma leading sample and (d) the grayscale image of melanoma leading lesion.

Using the same algorithm, the color variation ratios of all the 20 melanoma leading and benign mole samples are calculated and shown in Table 3-3. Table 3-3 also gives the mean and SD values in each group. As expected, the mean value of the color variation ratio in the melanoma leading is 120% larger than that in the benign group (0.494 vs. 0.224). Figure 3-13 plots the results and shows overlapping between the two groups. One can again identify the cutoff color variation ratio as 0.334, indicated by the non-overlapping ranges shown in the figure. The confidence of distinguishing a mole from a melanoma leading lesion using this cutoff ratio is 72.87%.

Table 3-3 Normalized color variation ratio for melanoma leading and benign mole samples.

Sample No.	Melanoma	Benign Mole
1	0.55967	0.37719
2	0.67301	0.18095
3	0.34337	0.15467
4	0.56314	0.33119
5	0.6181	0.165865
6	0.31906	0.30519
7	0.38434	0.095643
8	0.68308	0.35046
9	0.27413	0.15024
10	0.51834	0.12836
Mean	**0.494**	**0.224**
STD	**0.144**	**0.099**

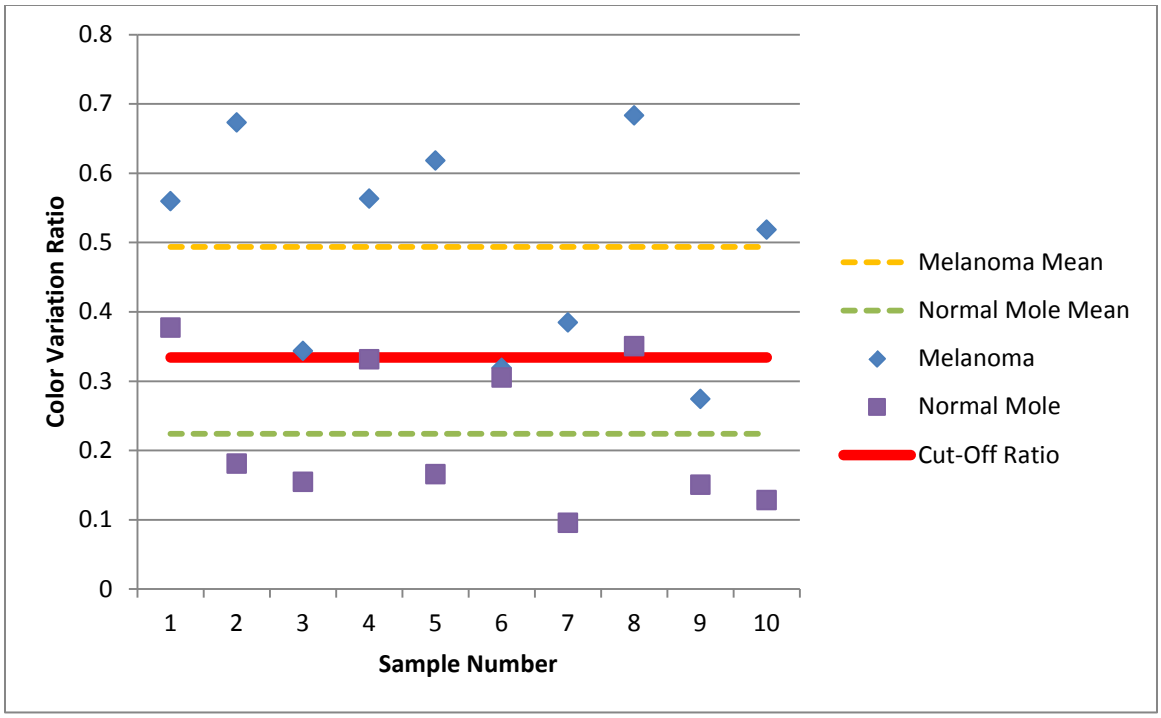

Figure 3-13 Comparison of melanoma leading and benign mole color variation ratios.

3.6 Mole Samples Provided by the Dermatologist

In this section, mole images taken by a dermatologist are analyzed using the same algorithms. Note that those images do not reflect mole images in general populations, and they represent images selected by the dermatologist, who visually identifies these moles as "irregular" in some aspects. Therefore, it will not be surprised to us if the calculated ratios already imply "leaning to" melanoma. At the time of this study, biopsies have not been performed to diagnose whether these moles are melanoma or not.

These images provided represent their initial images and the images of the same mole 6 or 12 months later. The main reason to include those images in our analyses is to provide quantitative measures to dermatologists to assess changes of those ratios over

time. It can also be used to validate the perspectives of dermatologists' presumed changes of a mole image over a period of time. Note that all the images are taken following the same photographic procedures and the light intensity, pixel size, and the image size are kept the same for all the images.

We first calculate the irregularity ratios of the images of those two groups. The results are listed in Table 3-4, and plotted in Figure 3-14. One notices that all the images have their irregularity ratio (3.23 or 3.25) much larger than the cutoff irregularity ratio identified in the previous section (cutoff ratio = 1.96). This is not a surprise since that may be the reason the dermatologist selected them for further analyses or tests. Among the ten moles, 4 moles' boundaries becomes more irregular over time, indicated by the positive values of the variation percentage in Table 3-4, while the other six moles appear less irregular on their borders over time than that of the initial images. The mean change of the irregularity ratio is 0.20%, however, if one calculates the absolute percentage change of the irregularity ratio, it is 8.79%±6.27% (mean±SD).

Table 3-4 Comparison of the irregularity ratios of the ten moles from their initial images to their images six or twelve months later.

Sample No.	Initial	Final	Variation Percentage	Absolute Change
1	3.7811	3.3927	-10.27%	10.27%
2	3.8468	3.9669	3.12%	3.12%
3	4.1696	4.6966	12.64%	12.64%
4	2.5545	2.762	8.12%	8.12%
5	3.2645	3.0784	-5.70%	5.70%
6	2.3871	2.3026	-3.54%	3.54%
7	2.4975	2.0513	-17.87%	17.87%
8	2.5644	2.5065	-2.26%	2.26%
9	2.9344	3.5533	21.09%	21.09%
10	4.3025	4.1596	-3.32%	3.32%
Mean	**3.23**	**3.25**	**0.20%**	**8.79%**
SD	**0.70**	**0.82**	**10.80%**	**6.27%**

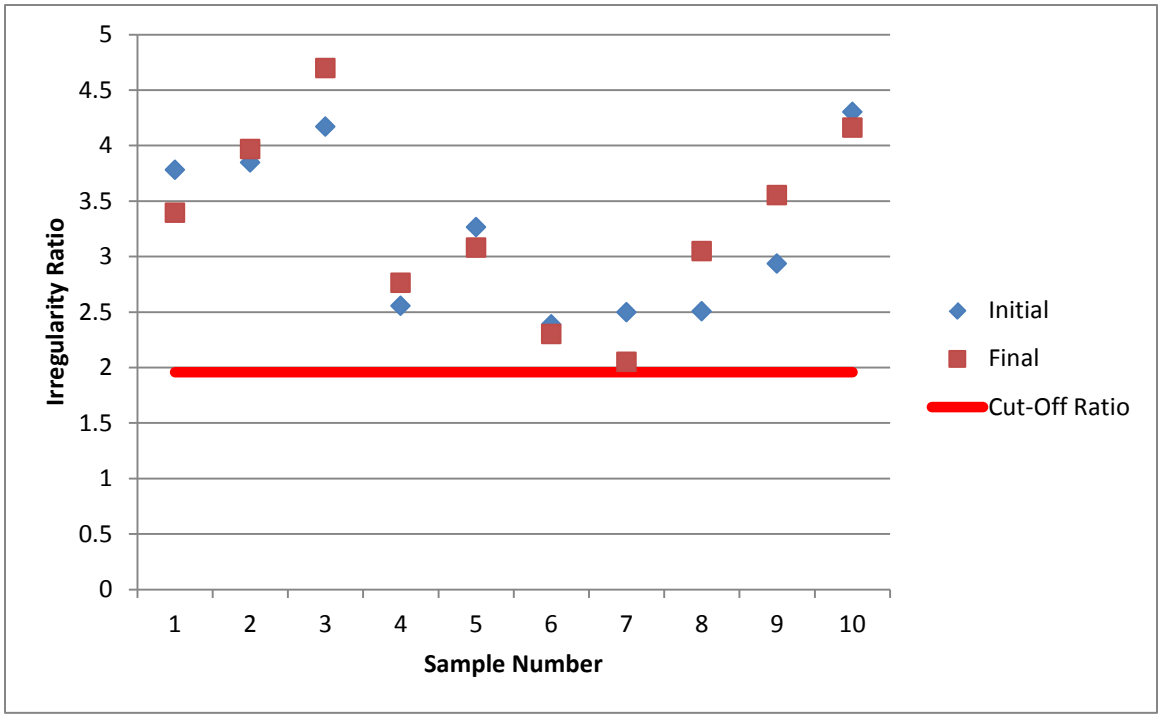

Figure 3-14 Irregularity ratios for the ten moles of their initial images and images six or 12 months later. Note that the cutoff irregularity ratio is 1.96, indicated by the bold red line.

Similar trends can be observed when one assesses the changes of the asymmetry ratios over time. The results are listed in Table 3-5 and illustrated in Figure 3-15. Almost all the asymmetry ratios are higher than the cutoff asymmetry ratio identified in the previous section. Again, the absolute percentage change over time is calculated as 9.13%±6.54%, with the largest change over 18%.

Table 3-5 Variation percentages in normalized asymmetry ratios for the initial and final sets of the mole images.

Sample No.	Initial	Final	Variation Percentage	Absolute Change
1	0.2225	0.2234	0.40%	0.40%
2	0.16482	0.15694	-4.78%	4.78%
3	0.26474	0.24512	-7.41%	7.41%
4	0.13947	0.16228	16.35%	16.35%
5	0.14579	0.14993	2.84%	2.84%
6	0.13648	0.11945	-12.48%	12.48%
7	0.10748	0.12107	12.64%	12.64%
8	0.190786	0.19058	-0.11%	0.11%
9	0.19132	0.22088	15.45%	15.45%
10	0.22857	0.18563	-18.79%	18.79%
Mean	**0.179**	**0.178**	**0.41%**	**9.13%**
SD	**0.047**	**0.041**	**11.22%**	**6.54%**

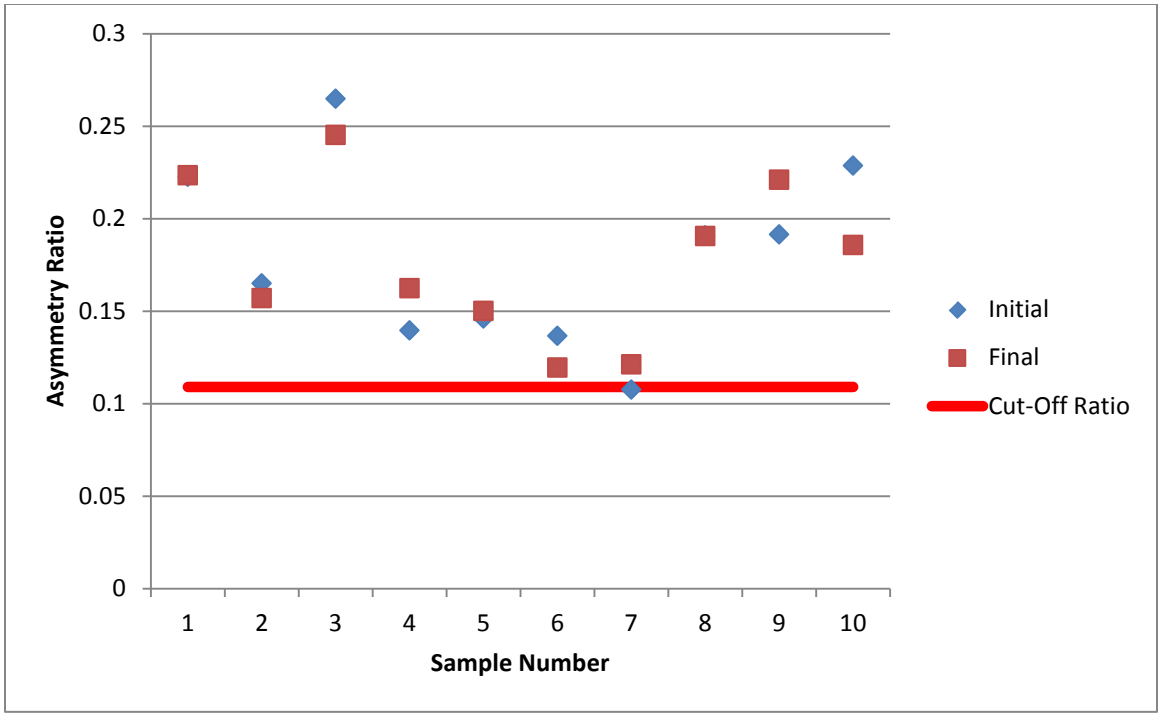

Figure 3-15 Comparison of the initial values and the final values of the asymmetry ratios of the ten mole samples. The cutoff asymmetry ratio identified in the previous section is represented by the bold red line.

It is a surprise to see that almost all the color variation ratios are below our cutoff color variation ratio of 0.334. The average values of the color variation ratio in both groups are 0.141 and 0.162, respectively. One possible reason is that our algorithm filters the color components. Nevertheless, our computational results indicate large changes in the color variation ratios over time. As shown in Table 3-6, 8 of the 10 moles appear having more grayscale variations over time, i.e., up to 81%. For the only two moles having a "negative" variation percentage, the percentage changes are less than 14%. The calculated absolute variation percentage and its standard deviation are 23.58%±21.45%.

Table 3-6 Variation percentages in normalized color variation ratios for the initial and final sets of the mole images.

Sample No.	Initial	Final	Variation Percentage	Absolute Change
1	0.10169	0.11655	14.61%	14.61%
2	0.097548	0.11447	17.35%	17.35%
3	0.067674	0.12267	81.27%	81.27%
4	0.21834	0.24898	14.03%	14.03%
5	0.14085	0.16289	15.65%	15.65%
6	0.24385	0.27736	13.74%	13.74%
7	0.25589	0.28914	12.99%	12.99%
8	0.13947	0.12871	-7.71%	7.71%
9	0.071374	0.10323	44.63%	44.63%
10	0.069093	0.059543	-13.82%	13.82%
Mean	**0.141**	**0.162**	**19.27%**	**23.58%**
SD	0.070	0.076	**25.39%**	**21.45%**

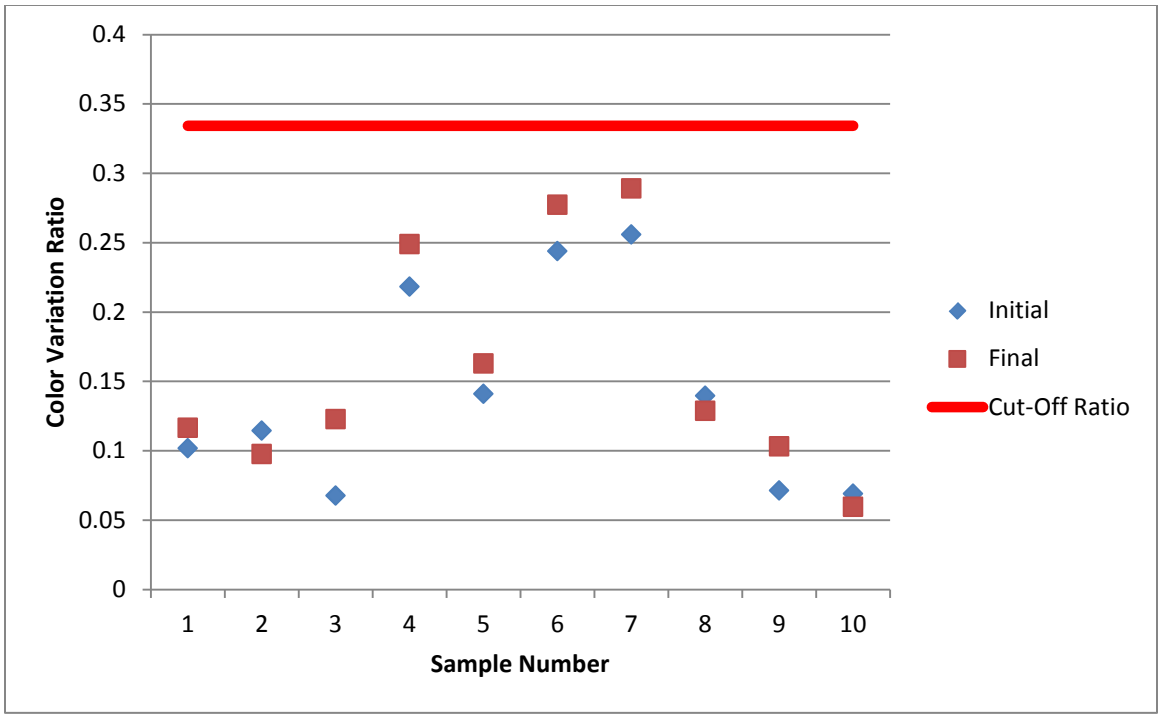

Figure 3-16 Comparison of the initial and final values of the color variation ratio over time. The cutoff color variation ratio is indicated by the bold red line.

Since the dermatologist can take the mole image over time under the same photographic conditions, one can track the size change of the mole, shown in Table 3-7 and Figure 3-17. Eight out of the ten moles have shown substantial increase in size. One mole (#9) has almost quadrupled its size. For the two moles which size is smaller after six months, the size decrease is very small, less than 6%.

Table 3-7 Variation percentages of the mole area (size) for the initial and final sets of the mole images. The size is represented by the total number of the pixels inside the mole.

Sample No.	Initial	Final	Variation Percentage	Absolute Change
1	53716	55600	3.51%	3.51%
2	88519	85674	-3.21%	3.21%
3	41144	45026	9.44%	9.44%
4	45258	55690	23.05%	23.05%
5	44760	57780	29.09%	29.09%
6	27645	35680	29.06%	29.06%
7	20046	28075	40.05%	40.05%
8	39081	41809	6.98%	6.98%
9	11694	43100	268.57%	268.57%
10	50802	48230	-5.06%	5.06%
Mean	**42266**	**49666**	**40.15%**	**41.80%**
SD	**20030**	**14913**	**77.47%**	**76.59%**

For some moles, not every ratio shows substantial changes over the period of six or twelve months. All the ten samples in this group were selected based on the dermatologist's subjective opinion that they have changed over time. We speculate that at least one of the ratios is substantial for him to assume that the mole is changing. Table 3-7 identifies the substantial changes of each mole among the four ratios. Here, we define "substantial changes" as ±14%. In doing so, it is clear that our eyes are most sensitive to the change in the color variation, followed by the size change. It is relatively difficult to assess changes over time in the border irregularity and/or the asymmetry of a mole.

Table 3-8 Substantial changes in the morphological ratios of all the 10 samples over time.

Sample	Irregularity Ratio	Asymmetry Ratio	Color Variation Ratio	Size Ratio
1	-	-	14.61%	-
2	-	-	17.35%	-
3	-	-	81.27%	-
4	-	16.35%	14.03%	23.05%
5	-	-	15.65%	29.09%
6	-	-	-	29.06%
7	-17.87%	-	-	40.05%
8	-	-	-	-
9	21.09%	15.45%	44.63%	268.57%
10	-	-18.79%	-	-

Sample 8 is an odd ball in the group since none of the ratios is higher than 8%. This is the only sample that our algorithm cannot validate the dermatologist's perception of change in the mole image. As shown in Figures 3-17a and 3-17b, it is indeed very difficult to make a decision whether the before and after images of mole #8 are different, except that the image is more blurred by observation. In the other nine moles, there is at least one ratio with a percentage variation change larger than 14%. For example, mole #9 has all four ratios larger than 14%. As shown in Figures 3-17c and 3-17d, there is a very large increase in size of this mole over time. When the size changes, on can see that mole #9 also shows substantial changes in its shape, leading to observed variations in its boundary irregularity and asymmetry. It becomes more patched over time, ending with an increase in the color variation ratio over time.

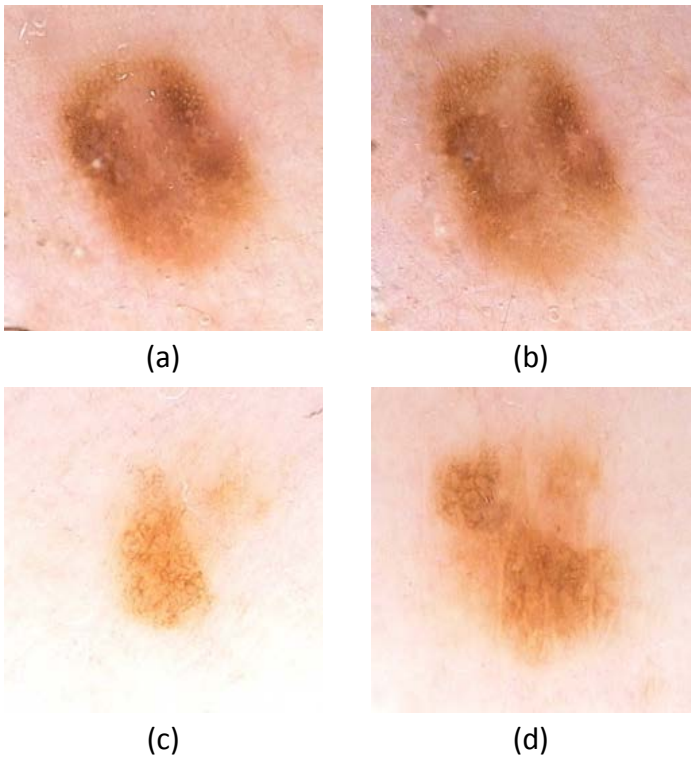

Figure 3-17 (a) The initial image of mole #8, (b) the image of mole #8 six months later, (c) the initial image of mole #9, and (d) the image of mole #9 six months later.

One thing we need to point out is that the definition of "substantial changes" as ±14% is arbitrary. If we select 7% as the definition of a substantial change, then all ten moles will have at least one ratio labeled as "being changed". Again, the sample size of the study is not very big to draw concrete conclusions. We just want to show that the developed algorithms have the potential to provide quantitative assessment of changes. When dermatologists screen a large number of moles in a patient, the algorithms can be used to assist the dermatologists to make decisions based on quantitative data rather than pure observation. This may be a very helpful tool for dermatologists with limited experience, as well as for primary physicians to decide whether to refer the patient to a specialist.

Chapter 4

Summary and Future Work

4.1 Summary

This thesis research is focused on advancing the image processing techniques and algorithms used for detecting skin melanoma based on photos taken from regular cameras and cellphones. We have modified previous image processing approaches and developed computational algorithms for quantifying morphological features of a mole image. Applying the algorithms to 20 mole images downloaded from educational websites, we have identified three cut-off ratios to distinguish melanoma images from benign mole images. The irregularity ratio cutoff is 1.96, suggesting 96% more circumference length than that of a circle with the same area. One finds that the cut-off ratio for assessing asymmetry of the mole image is 0.109, representing the degree of asymmetry as approximately 11%. Evaluation of the color variation of the moles leads to a cut-off ratio of the color variation as 0.334. Statistical analyses have been performed to determine the confidence of cut-off ratios, varying from 63% to 81%, for placing a mole image into its correct group. The algorithms have also been implemented to assess "changes" of mole images over time observed by a dermatologist. Using a ±14% as the definition of "substantial changes", the algorithm identifies 9 of the 10 mole images as changed over time. Among the irregularity, asymmetry, color variation, and size ratios, 5 out of the 9

moles have shown changes in one ratio, 2 out the 9 moles have experience changes in two ratios, 1 mole has shown changes in three ratios, and only 1 mole shows changes in all four ratios. The computational results are consistent with the general observations that human eyes are sensitive to size changes and color variation changes, and may not be very good to distinguish changes in border irregularity and asymmetry.

4.2 Contributions

Human eyes are very good at forming an impression on the size, color variation, asymmetry, and border irregularity. When it comes to quantified features such as "how irregular is the boundary of an image?" or "how symmetrical an image is?" human impression is not sufficient to determine the magnitude of these measures. It is why training is needed to distinguish subtle changes of those morphological features of an image. Typically, a dermatologist is better than a primary physician to make a quick decision whether a mole has an irregular shape, and whether the same mole changes over time based on looking at two images. The evaluation process may become tedious and subjective, leading to unnecessary biopsies or missing early Signs of a melanoma leading lesion is changes in size, shape or color of an existing mole.

A digital image has several properties that can be easily measured and quantified without any human input, therefore, minimizing inaccuracy due to subjective impression of the observer. Those properties include image sizes, number of pixels, the average color value of the image, histogram, etc. The computational algorithms developed in this study make it possible to produce an objective measurement of specific morphological

properties of an image that have been considered having connections with melanoma developments. Based on previous approaches of image processing procedures, we have developed in-house MATLAB codes that will automatically process the images, and calculate the three ratios associated with morphological features of mole images. Using the developed MATLAB codes, one can measure the extents of the boundary irregularity, asymmetry, color structure, and size of a mole image with no subjective input from the user. This can also pave a way to future development of a smartphone "app" based on automatic image processing calculations.

The developed computational algorithms have been used to assess human observation of "substantial changes" in mole images. Most dermatologists and primary physicians usually follow up certain moles over time. The current technology also allows them to photograph a mole with the same setting for easy comparison. The results from the computational algorithms have been shown to be consistent with human perception of obvious changes such as color variation and size. It also can be helpful to assist a physician in evaluating subtle changes that may not be very sensitive to the eyes. For example, boundary irregularity and asymmetry of a mole image may not be very evident to an observer. In fact all the moles selected by the dermatologist have their boundary irregularity and asymmetry ratios way above the cut-off ratios of those two groups. In other words, the boundary irregularity and asymmetry have to be very severe for a human observer to detect them. Therefore, the developed computational algorithms are useful in detecting those moles with boundary irregularity and asymmetry ratios above the cutoff ratios, however, below the thresholds of human eye detection.

As discussed in the introduction section, melanoma can be treated easily in its early stages. However, a professional diagnosis of melanoma involves multiple steps, including making an appointment with the dermatologist, taking a day off to see the doctor, biopsy, etc. This process is time consuming. If asking around, one may find that most of us have not seen a dermatologist for more than 10 years. We believe that the developed computational algorithm would prompt the general population to at least make an appointment with their dermatologist based on the calculated ratios. Nowadays, smartphones are incredibly popular and widely used by the public. The general population can use their smartphone to take a picture of a mole, and then submit it to our website via an app. The three ratios can be calculated right way and sent back to the user. All of those can be done in a private and quiet setting. If the ratios are way above the cutoff thresholds, the user can be prompted to a list of local dermatologists to make an appointment. Even though the ratios calculated by the smartphone app may not be regarded as a professional diagnosis, it can urge the general population to see their dermatologist for further screening. The algorithms and its future smartphone app can also be used as effective tools for melanoma educations and awareness.

4.3 Limitations and Future Work

This study is limited by a very small sample size included in the study. The cutoff ratios identified are all based on the small sample size of 10 moles in each group. In addition, the ten moles in each group may not well represent the actual mole images one may observe on his/her skin, since they have been screened and selected by the

physicians to illustrate the difference between benign moles and melanomas. In reality, the difference between them may be more blurred than what our results indicate. Consequently, the confidence from statistical analyses may also require modification if the sample size is bigger. Future collaboration with dermatologists who have access to mole image samples will be helpful. In addition, positive or negative diagnoses of melanomas via biopsy or other approaches can be used to confirm how good the computational tools in predicting the outcomes.

We have found out that another limitation of the study is on the uncertainty of the boundary irregularity ratio calculations. Currently, a smartphone image can have a very high resolution, leading to a very small pixel size on a digital image. Since the boundary of a mole image is represented by discrete vertical and horizontal pixel segments, it is possible that the small segments actually overestimate the irregularity of the boundary. In another word, the original smooth boundary line is represented by connecting many small vertical and horizontal pixel segments. Note that we only generate a circular shape with the same area under the same pixel resolution. In theory, the same thing also occurs on boundary of the circular shape. It is expected that the irregularity ratio defined as the ratio of the total boundary pixels of a mole to that of a circular shape with the same area, would have eliminate the uncertainty. Future research can be performed to test the sensitivity of our calculated irregularity ratio to the image resolution, especially the resolution is very high.

In this study, the mole images are converted to grayscale for calculating the ratios. This conversion should not affect the calculations of the boundary irregularity and asymmetry ratios; however, it may affect the color variation ratio. A color pixel is

associated with a combination of three distinct numbers, each representing the magnitude of color “red”, “green”, and “blue”. By converting a color pixel to grayscale, we will end up with only one grayscale value with a 0-255 range, hence eliminating a huge amount of data associated with color. Further studies on development of computational algorithms based on color pixel are warranted.

References

[1] M. Saraiya, K. Glanz, P. A. Briss, P. Nichols, C. White, D. Das, *et al.*, "Interventions to prevent skin cancer by reducing exposure to ultraviolet radiation: A systematic review," *American Journal of Preventive Medicine,* vol. 27, pp. 422-466, 12// 2004.

[2] A. L. Chan Agero, K. J. Busam, C. Benvenuto-Andrade, A. Scope, M. Gill, A. A. Marghoob, *et al.*, "Reflectance confocal microscopy of pigmented basal cell carcinoma," *Journal of the American Academy of Dermatology,* vol. 54, pp. 638-643, 4// 2006.

[3] K. J. Busam, C. Charles, C. M. Lohmann, A. Marghoob, M. Goldgeier, and A. C. Halpern, "Detection of intraepidermal malignant melanoma in vivo by confocal scanning laser microscopy," *Melanoma Research,* vol. 12, 2002.

[4] M. C. Staff. (2002). *Melanoma* [Web Site]. Available: http://www.mayoclinic.org/diseases-conditions/melanoma/basics/definition/con-20026009

[5] S. C. Foundation. (2005). *What Is Melanoma*. Available: http://www.skincancer.org/skin-cancer-information/melanoma

[6] N. C. Institute. (2005). *Melanoma*. Available: http://www.cancer.gov/cancertopics/types/melanoma

[7] A. C. Society. (02/20/2014). *What are basal and squamous cell skin cancers?* Available: http://www.cancer.org/cancer/skincancer-basalandsquamouscell/detailedguide/skin-cancer-basal-and-squamous-cell-what-is-basal-and-squamous-cell

[8] M. McCusker, N. Basset-Seguin, R. Dummer, K. Lewis, D. Schadendorf, A. Sekulic, *et al.*, "Metastatic basal cell carcinoma: Prognosis dependent on anatomic site and spread of disease," *European Journal of Cancer,* vol. 50, pp. 774-783, 3// 2014.

[9] C. Jhappan, F. P. Noonan, and G. Merlino, "Ultraviolet radiation and cutaneous malignant melanoma," *Oncogene,* vol. 22, pp. 3099-3112, //print 0000.

[10] T. S. Housman, "Skin cancer is among the most costly of all cancers to treat for the Medicare population," *J Am Acad Dermatol,* vol. 48, pp. 425-429, // 2003.

[11] R. Marks, "Imiquimod 5% cream in the treatment of superficial basal cell carcinoma: results of a multicenter 6-week dose-response trial," *J Am Acad Dermatol,* vol. 44, pp. 807-813, // 2001.

[12] T. P. R. Group. *Melanin, melanocytes, and melanosomes*. Available: http://palaeo.gly.bris.ac.uk/melanosomes/melanin.html

[13] *Is It Melanoma*. Available: http://www.melanoma.org/understand-melanoma

[14] *Types of Melanoma*. Available: http://www.skincancer.org/skin-cancer-information/melanoma/types-of-melanoma

[15] *Cutaneous Melanoma, or Melanoma of the Skin*. Available: http://www.melanoma.org/understand-melanoma/what-is-melanoma/cutaneous-melanoma

[16] Z. Kutlubay, B. Engin, S. Serdaroğlu, and Y. Tüzün, "Current Management of Malignant Melanoma: State of the Art," 2013.
[17] *Lentigo Maligna*. Available: http://flexikon.doccheck.com/de/Lentigo_maligna
[18] *Acral Lentiginous*. Available: http://stanfordmedicine25.stanford.edu/the25/hand.html
[19] *Nodular Melanoma*. Available: http://library.bjmu.edu.cn/pbl/sdxm/evident/neoplasms/mdx_20.htm
[20] *Melanoma Statistics*. Available: http://seer.cancer.gov/
[21] *Cancer Statistics*. Available: http://www.cancer.org/cancer/skincancer-melanoma/detailedguide/melanoma-skin-cancer-key-statistics
[22] *Cancer Facts & Figures*. Available: http://www.cancer.org
[23] J. Chen, "Cost of nonmelanoma skin cancer treatment in the United States," *Dermatol Surg,* vol. 27, pp. 1035-1038, // 2001.
[24] D. E. Rowe, "Prognostic factors for local recurrence, metastasis, and survival rates in squamous cell carcinoma of the skin, ear, and lip: implications for treatment modality selection," *J Am Acad Dermatol,* vol. 26, pp. 976-990, // 1992.
[25] *Causes for Melanoma*. Available: http://www.skincancer.org/prevention/are-you-at-risk
[26] J. C. Martinez and C. C. Otley, "The management of melanoma and nonmelanoma skin cancer: a review for the primary care physician," *Mayo Clin Proc,* vol. 76, pp. 1253-1265, // 2001.
[27] J. A. Neville, E. Welch, and D. J. Leffell, "Management of nonmelanoma skin cancer in 2007," *Nat Clin Prac Oncol,* vol. 4, pp. 462-469, 08//print 2007.
[28] *Melanoma Prevention Methods*. Available: http://www.skincancer.org/skin-cancer-information/melanoma/melanoma-prevention-guidelines
[29] A. Chakrabarty and J. Geisse, "Medical therapies for non-melanoma skin cancer," *Clin Dermatol,* vol. 22, pp. 183-188, // 2004.
[30] "Melanoma Diagnosis," ed: American Cancer Society.
[31] M. Thissen, "A systematic review of treatment modalities for primary basal cell carcinomas," *Arch Dermatol,* vol. 135, pp. 1177-1183, // 1999.
[32] D. E. Rowe, "Long-term recurrence rates in previously untreated (primary) basal cell carcinoma: implications for patient follow-up," *J Dermatol Surg Oncol,* vol. 15, pp. 315-326, // 1989.
[33] C. A. Morton, "Photodynamic therapy for large or multiple patches of Bowen's disease and basal cell carcinoma," *Arch Dermatol,* vol. 137, pp. 319-324, // 2001.
[34] N. Voss and C. Kim-Sing, "Radiotherapy in the treatment of dermatologic malignancies," *Dermatol Clin,* vol. 16, pp. 313-320, // 1998.
[35] K. Korotkov and R. Garcia, "Computerized analysis of pigmented skin lesions: a review," *Artificial intelligence in medicine,* vol. 56, pp. 69-90, 2012.
[36] *Sobel Operator*. Available: https://en.wikipedia.org/wiki/Sobel_operator
[37] Z. Zhang, W. V. Stoecker, and R. H. Moss, "Border detection on digitized skin tumor images," *Medical Imaging, IEEE Transactions on,* vol. 19, pp. 1128-1143, 2000.
[38] J. E. Golston, W. V. Stoecker, R. H. Moss, and I. P. Dhillon, "Automatic detection of irregular borders in melanoma and other skin tumors," *Computerized Medical Imaging and Graphics,* vol. 16, pp. 199-203, 1992.

[39] W. V. Stoecker, W. W. Li, and R. H. Moss, "Automatic detection of asymmetry in skin tumors," *Computerized Medical Imaging and Graphics,* vol. 16, pp. 191-197, 1992.
[40] S. V. Patwardhan, A. P. Dhawan, and P. A. Relue, "Classification of melanoma using tree structured wavelet transforms," *Computer methods and Programs in Biomedicine,* vol. 72, pp. 223-239, 2003.
[41] G. Monheit, A. B. Cognetta, L. Ferris, H. Rabinovitz, K. Gross, M. Martini*, et al.*, "The performance of MelaFind: a prospective multicenter study," *Archives of dermatology,* vol. 147, pp. 188-194, 2011.
[42] *MelaFind*. Available: http://melasciences.com/melafind
[43] *Aura Scanner*. Available: http://www.verisante.com/
[44] R. Szeliski, *Computer vision: algorithms and applications*: Springer, 2010.
[45] X. Mei, Z. Zheng, W. Bingrong, and L. Guo, "The edge detection of brain tumor," in *Communications, Circuits and Systems, 2009. ICCCAS 2009. International Conference on*, 2009, pp. 477-479.
[46] R. Garnavi, M. Aldeen, M. E. Celebi, G. Varigos, and S. Finch, "Border detection in dermoscopy images using hybrid thresholding on optimized color channels," *Computerized Medical Imaging and Graphics,* vol. 35, pp. 105-115, 2011.
[47] M. E. Celebi, H. Iyatomi, G. Schaefer, and W. V. Stoecker, "Lesion border detection in dermoscopy images," *Computerized Medical Imaging and Graphics,* vol. 33, pp. 148-153, 2009.
[48] H. Iyatomi, M. E. Celebi, G. Schaefer, and M. Tanaka, "Automated color calibration method for dermoscopy images," *Computerized Medical Imaging and Graphics,* vol. 35, pp. 89-98, 2011.
[49] L. He, L. R. Long, S. Antani, and G. R. Thoma, "Histology image analysis for carcinoma detection and grading," *Computer methods and programs in biomedicine,* vol. 107, pp. 538-556, 2012.